12-3-2019

Investigation and Characterization of PC12 Cells Adhesion, Proliferation, and Regeneration on Aerogels as a function of Topography and Stiffness.

Martina Rodriguez Sala

INVESTIGATION AND CHARACTERIZATION OF PC12 CELLS ADHESION, PROLIFERATION, AND REGENERATION ON AEROGELS AS A FUNCTION OF TOPOGRAPHY AND STIFFNESS

by

Martina Rodriguez Sala

A Thesis

Submitted in Partial Fulfillment of the

Requirement for the Degree of

Master of Science

Major: Physics

The University of Memphis

December 2019

Acknowledgments

I want to thank Dr. Firouzeh Sabri for the advisor role she has done over the last few years. I would also like to thank Dr. Omar Skalli for his support and allowing me to use the cell culture room in his laboratory. Thank you to my committee members Dr MS Jahan, Dr O Skalli, and Dr C Peng for providing comments and feedback on my work.

I want to thank Dr. Chenhui Peng for his work regarding the plasmonic photo-patterning of glass and aerogels.

I would like to acknowledge Dr. Nicholas Leventis for providing the Memory Shape Polymer Aerogels.

I would like to acknowledge Dr. Marcus Worsley for providing the Carbon Aerogels used in this study.

Thank you to the students that have worked in Dr. Sabri's lab over the past years as well as Kyle Lynch for his numerous help and mentorship.

Abstract

Limitations with existing methods and materials used for nerve repair shows the significant interest to keep researching new materials for nerve implants. Recent studies show the importance of material properties to cell behavior. This body of work focuses on understanding the effect of material properties on the behavior of PC12 neurons. The first part of the work attemepts to quantify the relationships between cell parameters and substrate properties. Based on this study, random topographies with surface roughness of 0.5 μm and Young's modulus of 2MPa are the optimum substrates for neurite outgrowth in PC12 cells. The second part investigates the feasibility of creating precise patterns on aerogel susbtrates for alignment by means of plasmonic photopatterning techniques. Those results have shown a degree of alignment in neurites due to the continuous topography.

Table of Content

List of Figures

List of Symbols and Abbreviations

NGF	Nerve Growth Factor
ECM	Extra Cellular Matrix
SCD	Supercritical Drying
PDMS	Polydimethylsiloxane
PCSA	Polyurea Crosslinked Silica Aerogel
CA	Carbon Aerogel
BRF-CA	Base-Catalyzed Resorcinol Formaldehyde Carbon Aerogel
ARF-CA	Acid-Catalyzed Resorcinol Formaldehyde Carbon Aerogel
MSPA	Memory Shape Polymer Aerogel
TCPS	Tissue Culture Polystyrene
Sa	Arithmetic mean of the absolute height
WLI	White-light interferometry
LC	Liquid Crystal
ES	Electrical Stimulation
P_{ij}	Dipole strength
u_{ij}^{e}	Strain of the environment
r_c	Cell position
W	Work
F	Force
K	Spring Constant
η	Viscosity of the solvent
ρ'	Density of the colloidal particles
ρ	Density of solvent
P	Capillary pressure or tension
γ_{LV}	Liquid and vapor interfacial tension
θ	Contact area
r	Pore radius
PD	Path difference
E	Young's modulus
σ	Stress
ε	Strain
F	Force
A	Area
dL	Elongation
L	Length

Chapter 1. Introduction

1.1 Nervous System

The nervous system is a complex network with two interconnected parts. The central nervous system (CNS) oversees the processing of information, and the peripheral nervous system (PNS) is in charge of transmitting data between the body and the central nervous system [1]. Neurons are the cells specialized to carry this information in the form of electrical signals using unique structures such as dendrites and axons [2]. Nerves are bundles of axons that can be damaged preventing the flow of information throughout the nervous system. This kind of injury can result in life-defining consequences such as the loss of sensory and mobility capacities [3]. A key feature that differentiates the peripheral from the central nervous system is that the PNS has a higher regenerative capacity than the CNS [4, 5].

1.1.1 Nerve Injuries

After an injury, the nerve may react in different ways. Wallerian degeneration is the process that occurs after an axon is severed. This process degrades the entire nerve distal direction from the cell body [6]. This process occurs without damaging the cell body of the neuron, which ensures its regeneration afterward [7]. After Wallerian degeneration, Schwan's cells proliferate, forming a column that provides a pathway for the axonal regeneration [8]. The Growth cone is a specialized structure built by lamellipodium and filopodia that helps nerves regenerate. This structure explores the extracellular environment to determine the direction of the growth using biochemical and physical cues [9].

1.1.2 Nerve Regeneration

There are twenty million Americans that suffer from peripheral nerve injuries (PNI), which results in $150 billion in annual health-care [10, 11]. Even though regeneration occurs

naturally, it is at a slow rate; the best outcomes suggest 1-2mm/day [12]. The timeframe for reinnervation is not infinite [13, 14]. In summary, peripheral nerve injuries are a standard incidence in humans. They cause the loss of motor, sensory, or autonomic function in the denervated body part leading to severe functional impairment as well as muscle atrophy [5, 15].

1.1.3 Current Peripheral Nerve Repair Techniques

There are multiple techniques to speed up the process of peripheral nerve repair; epineural microsutures, grafts, and laser nerve welding. Epineural microsutures is a common technique that directly repairs the nerves with a surgical treatment that sutures the two ends of a fractured nerve together [16]. Grafts are a surgical practice used when there is a gap between the nerve ends. The nerve ends are joined by a section of another nerve [17]. Nerve grafting can be divided into autographs and allograft depending if the nerve used to replace the injury is from the same patient or a donor. Laser nerve welding is a technique that uses the thermal heating of a laser beam and subsequent cooling to repair the nerves. It avoids the introduction of foreign materials into the injury [18]. There have been multiple technological advances in the last years, but the complete recovery of nerve function is hardly ever accomplished [16]. It is essential to keep researching peripheral nerve repair and regeneration to find a way to achieve a better recovery after nerve trauma [19].

1.2 Response of neurons to their surroundings

Limitations with existing methods and materials used for nerve repair necessitate the design and characterization of novel biomaterials. Such techniques should enhance the desired neural responses and functionality. Artificial nerve guidance conduits developed as an alternative way to repair peripheral nerve injury still cannot obtain satisfactory prognosis in clinical settings.

Nervous tissue, both central and peripheral, is formed by a complex three-dimensional environment with a wide range of topographies, morphologies, and sizes. When studying novel techniques for nerve regeneration, the factors that can be considered are biochemical signals, material properties, and external stimuli. Various studies have focused on the biochemical signals that influence cell behavior, but recently there has been a rise in how physical parameters affect cells [20]. These physical parameters are material properties of biomaterials that can be modified and tuned to meet specific requirements for tissue regeneration and regulate cell behavior [21]. Physical parameters that have been studied include substrate roughness and Young' modulus.

1.3 PC12 Cells as Neuronal Analogs

In vitro studies are the starting point to investigate the cell behavior in neural cells, which can then be translated into *in vivo* assays and clinical neuroscience. When working *in vitro,* cell culture is used. Cell cultures are the removal of cells from an animal or plant to be grown in an artificially controlled environment [22]. Primary cell culture can be differentiated from secondary cell culture. Primary cell culture cells are obtained directly from animal tissue. On the other hand, in secondary cell culture, the cell line is already disassociated from tissue. Secondary cell culture allows the proliferation of cells in laboratory conditions [23]. There are drawbacks and advantages to both types of cell cultures, and there needs to be a basic understanding of those differences. For example, secondary cells are cost-effective and easy to reproduce, but their behavior might not be exactly as those of primary cells [24]. Current studies use the hippocampus or cortex cells for the CNS and Dorsal root ganglia (DRG) and superior cervical ganglia (SCG) as primary cells. As a secondary cell line, PC12 cells have been widely used.

PC12 cells are a useful model for neurobiological and neurochemical studies of the peripheral nervous system [25, 26, 27, 28, 29, 30, 31, 32, 33]. PC12 cells are a cell line obtained for a white rat pheochromocytoma cancer cells [25]. In the absence of NGF, cells have round or ovoid shapes and form small clusters of cells and proliferate. With the introduction of nerve growth factor (NGF), PC12 cells stop proliferating and start growing extensions, giving the second type of phenotype. Moreover, PC12 cells have a homogeneous cell chromosome. It suggests that the cell line will remain genotypically and phenotypically stable *in vitro* for many generations [34].

1.4 Introduction to aerogels

Aerogels are an attractive class of mesoporous materials with tunable chemical, physical, bulk, and surface properties. Aerogels have a wide range of applications, from aerospace to biomedical applications, due to their excellent features such as their incredibly high porosity, low density, etc. [35]. Aerogels have great potential for biomedical applications such as drug delivery [36], cardiovascular implantable medical devices [37], tissue engineering [38], and wound care applications [39]. Moreover, recent studies show the potential for this material for *in vivo* and *in vitro* studies [40, 41, 42, 32]. Aerogels were presented by Kistler in 1932 to refer to those gels for which the liquid was exchanged with gas without collapsing its nanostructure of a pearl-like network of particles [43]. Aerogels can be classified depending on their appearance, their microstructure, or their composition. According to their presence, aerogels can be described as monoliths, powders, or films. Based on the structure, aerogels can be classified as microporous (<2 nm), mesoporous (2-50 nm), and mixed-porous aerogels [44]. Most often, aerogels are sorted based on their composition, inorganic, organic, and inorganic-organic hybrid aerogels [35]. Of interest to this study, three different types of aerogels are described; Polyurea Crosslinked Silica

Aerogel (PCSA), Carbon Aerogel (CA), and Memory Shape Polymer Aerogel (MSPA). The different aerogels will be further discussed in chapter 3.

1.5 Research aims

The work presented here aims to build a pool of knowledge from which an aerogel scaffold could be used for peripheral nerve regeneration. Few studies have used aerogel as supportive scaffolds for nerve regeneration, and therefore an initial effort *in vitro* needs to be accomplished to assert the possibilities of this material. Moreover, the variety and tunable properties of aerogels allow for a better understanding of how material properties affect cell behavior. The research work presented here has different aims. First, to understand the impact of substrate topography on nerve-like cells *in vitro.* Various properties of cells are measured and compared between the different substrates. Second, to understand the effect of the substrate Young's modulus on nerve-like cells *in vitro*. Additionally, the introduction of a plasmonic photopatterned is added to PCSA to investigate cell behavior due to continuous topography.

1.6 Thesis Outline

The work presented here has been organized in the following manner: Chapter 2 reviews the theoretical background related to neural scaffolds, aerogels, PC12 cells, and the techniques used to measure surface roughness and stiffness. Chapter 3 discusses the materials used in this study, as well as the methods used to synthesize them. Chapter 4 shows the details and protocol followed to culture cells onto the different substrates. The different results obtained in this study are found in chapter 5. The first round of results focuses on the success rate in cell culture in each of the different aerogel substrates. The response of cells in the different aerogel substrates is then explained. The collagen behavior is later described and illustrated. The final two sections focused on the material properties of the aerogel substrates and the relationship between cell

response to those materials properties. Chapter 6 investigates the preliminary results of layering a continuous topography onto aerogel and the overall results regarding cell culture on it. The last chapter concludes this work.

Chapter 2. Theoretical Background

2.1 Biophysics of cell behavior

Cells adhere to the Extra Cellular Matrix (ECM) using focal adhesions, which uses actin micro-filaments and integrins. Focal adhesions interact with the proteins of the EMC [45]. This process is critical for cells to function correctly [46]. Focal points are made up of large quantities of proteins, more than sixty have been identified to be involved in focal adhesions. These proteins have catalytic roles as well as adaptor roles. Focal points allow the cell to attach to the ECM but also allow communication between the cell and its environment [47].

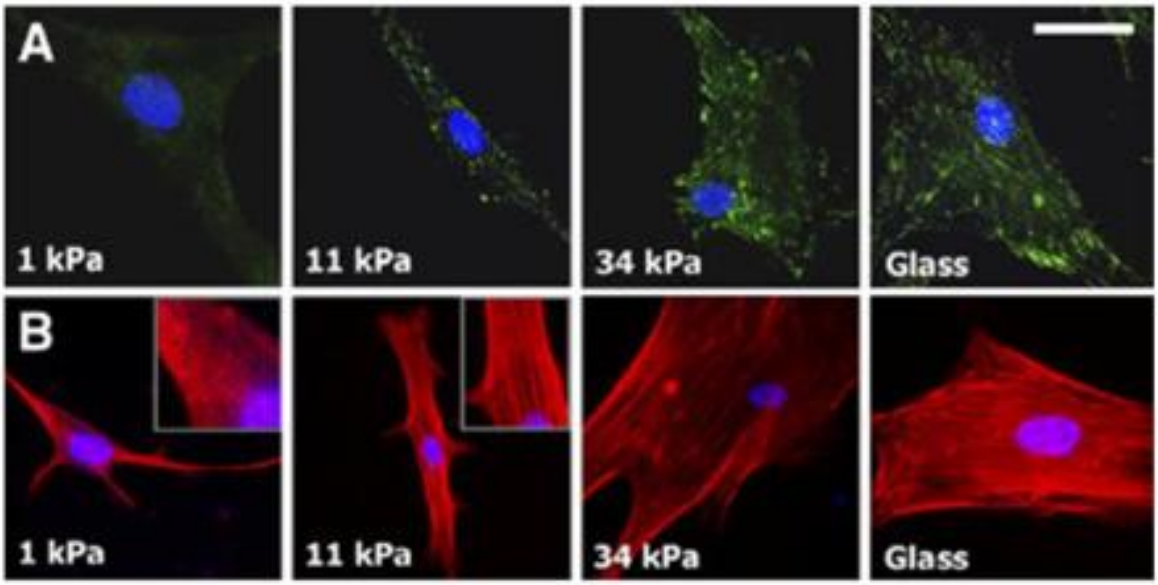

Figure 1: Cell attachment (a) Increased substrate stiffness induces the formation of focal adhesion complexes (green). (b) Increased substrate stiffness induces actin polymerization and alignment (red) in human mesenchymal stem cells **[48]**.

Moreover, cell shape is a consequence of the internal cytoskeletal process and adhesion molecules within the cell membrane that interacts with its surrounding [49]. Cell spreading and migration have been described using a model by Bischofs et al. This model uses Young's modulus and the Poisson ratio of the substrates. The cell-matrix contacts are coupled through the

actin cytoskeleton. This proposed model assumes that the work the cell actively pulls on its surrounding matrix is minimized;

$$\Delta W = P_{ij} u_{ij}^{e}(r_c) \tag{2.1}$$

Were P_{ij} is the anisotropic force contraction dipole described by

$$P_{ij} = P n_i n_j \tag{2.2}$$

where P is the dipole strength, *n* is its orientation at the cell position r_c , and u_{ij}^{e} is the strain of the environment. Moreover, the matrix is assumed to behave like a spring with a constant K, the work produced by the cell to produce a force for movement equals to:

$$W = \frac{F^2}{2K} \tag{2.3}$$

In isotropic substrates where the Young's modulus (E) is equal throughout the substrate, all Ks are equal, and the different focal adhesions act similarly. On the other hand, the forces in anisotropic substrates are various due to variance in Young's modulus throughout the substrate (E_1, E_2). Therefore, there is a directionality of the cell towards the maximal effective stiffness [50].

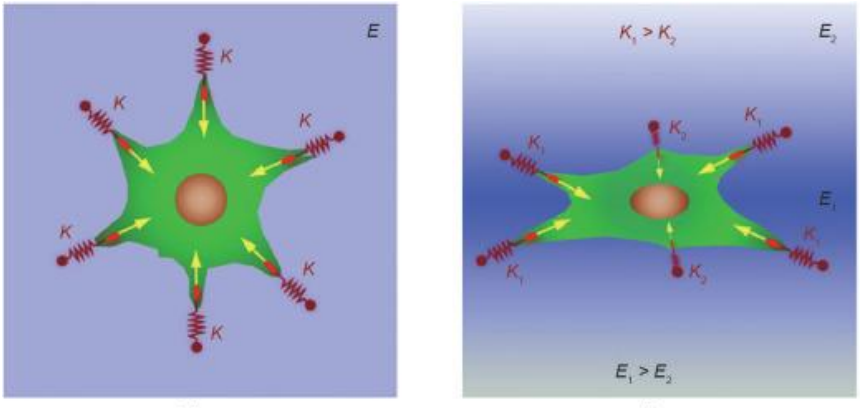

Figure 2: Local elasticity of the substrate is represented by spring constants K (a) In an isotropic matrix, were all constants are equal due to uniform young's modulus on the substrate (E). (b) In an anisotropic matric, where the forces are dependent on the local stiffness of the substrate (E_1, E_2) **[50]**.

2.2 Attachment of PC12 Cells

PC12 cells have been shown to attach poorly to surfaces that are not coated with proteins [25, 51]. Studies have shown how PC12 cell attachment increases when substrates are coated with laminin, collagen, and other extracellular matrix components [33, 27, 26, 52, 31]. To culture PC12 cells *in vitro*, the substrate needs to be coated with rat tail collagen I, before cell seeding [25].

2.3 Aerogels

Aerogels are an attractive class of mesoporous materials with tunable chemical, physical, bulk, and surface properties. They have great potential for in vitro and in vivo applications (e.g., scaffolds, artificial membranes, medical inserts, nerve repair conduits, etc.)

2.3.1 Mechanical Properties

Aerogels have characteristics such as: 90% porosity (resulting in densities as low as 0.003 g/cm3), highly open porous structure, (allowing the exchange of nutrients without interfering with the nerve cell), high mechanical strength, high surface-to-volume ratio (typically 600-1000 m2/g), and tolerance for chemical treatments [53]. Multiple techniques are used to investigate the mechanical properties of aerogel. Aerogels have an open pore network with an unusual combination of small pore size and high porosity. Porosity is described as the void space in a solid [54]. The basic technique used for aerogel porosity is nitrogen adsorption/desorption. The amount of adsorbed gas weight uptake and sample volume are used to measure porosity [55]. The porosity is defined as:

$$P_{adsorption} = \frac{V_{nitrogen}}{V_{solid}} \tag{2.4}$$

Where P is the porosity of the aerogel, $V_{nitrogen}$ is the volume of nitrogen adsorbed by the aerogel, and V_{solid} is the volume of the aerogel. The mechanical strength of aerogels is measured using three-point bending, uniaxial compression, or ultrasonic techniques [56].

2.3.2 Aerogel chemistry

A sol-gel process synthesizes aerogel. It is a wet-chemical technique consisting of the formation of a liquid sol phase into a solid gel phase divided by multiple steps; solution formation, gelation, aging, and drying [57]. The sol phase is formed by a uniform colloidal solution. The sedimentation rate of the colloidal particles can be understood using Stokes' law, assuming that the particles are spherical;

$$\frac{dx}{dt} = \left[\frac{\frac{4\pi r^3}{3}(\rho' - \rho)g}{6\pi r\eta}\right] = \left[\frac{2r\text{^}2(\rho' - \rho)g}{9\eta}\right] \tag{2.5}$$

Where η represents the viscosity of the solvent, r is the radius of the particles, ρ' is the density of the colloidal particles, and ρ is the density of the solvent [57]. With small solid particles, the van der Waals interactions dominate over the gravitational forces, and therefore the particles display Brownian motion [43]. Once the solution is formed, the gelation process occurs, where the sol is transformed into a gel phase that consists of a 3D continuous robust network enclosing a liquid phase [58]. The solid and liquid phases are linked within each other. The liquid does not allow the solid network to collapse, and the structural network does not allow the liquid to free flow [59]. Aging refers to the process in which the gel network is strengthened [57]. Multiple processes occur during aging. For example, the structure and properties of the gel will change due to the condensation of particles and monomers form the liquid phase into the existing network. Moreover, the contraction of the structure causes a spontaneous shrinkage due to the flexibility of the internal structure [58].

2.3.3 Gel drying

After gelation and aging, the next step consists in drying the gel. There are three different types of drying: air drying, supercritical drying (SCD), and freeze-drying. Depending on the technique used, the product obtained is different. Air drying of the gel cause shrinking and fracture due to capillary tension on the small pores. The nanostructure of the aerogel collapses due to this pressure forming a xerogel. The capillary tension or pressure can be described using Young-Laplace equations;

$$P = \frac{2\gamma_{LV}cos\theta}{r} \tag{2.6}$$

Where P is the capillary pressure, $\boldsymbol{\gamma_{LV}}$ represents the liquid and vapor interfacial tension, $\boldsymbol{\theta}$ is the contact angle, and r is the pore radius [58].

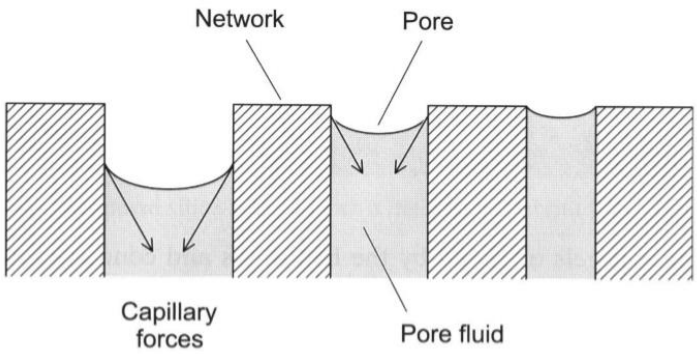

Figure 3: Diagram of capillary forces on small pores. Capillary forces on small pores cause collapsing of the internal aerogel structure when air drying **[58]**.

SCD is used to avoid the collapsing of the structure of the gel. This technique consists of increasing the temperature and pressure above the critical point of the liquid, transforming it into a supercritical fluid where each molecule can freely move without surface tension. Reaching the supercritical state allows the liquid to be separated from the gel network creating an aerogel. Freeze-drying involves freezing the solvent insides the 3D network of the gel as well as lowering

the pressure below sublimation to remove the solvent without the liquid-vapor interface. The product of this process may be called cryogels.

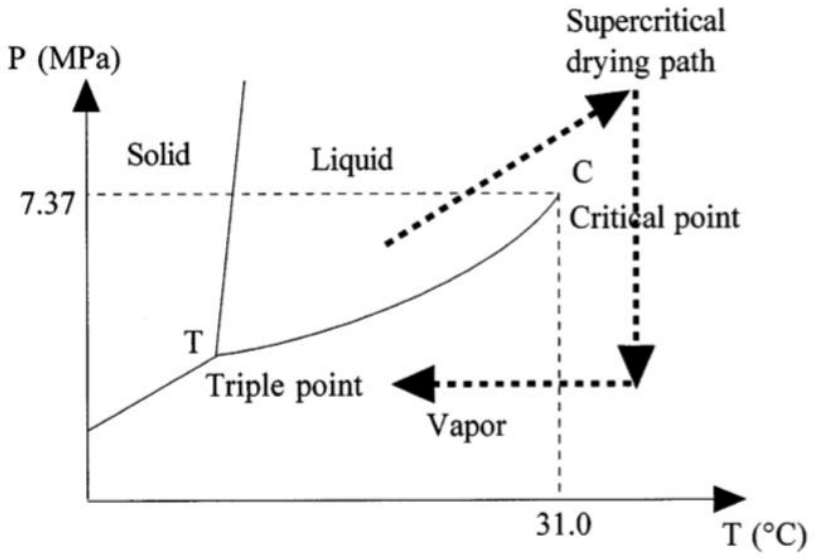

Figure 4: Phase diagram for SCD. Dotted arrows show the steps followed during supercritical drying to dry aerogels without collapsing their internal structure **[60]**.

2.4 Substrate topography

It has been shown that the attachment of cells to the extracellular matrix (ECM) not only allows for cell attachment but also communication within its surroundings. Therefore cells are spatially aware of the underlying topography of substrates they are attached to and respond differently depending on the type of topography [29, 61, 30, 62, 31]**.** Moreover, during nerve injury, Schwan's cells proliferate and organize in longitudinal cell columns called bands of Bungner. This structure serves as a substrate for regenerating peripheral nerves. This natural regeneration already points towards how important topography is during nerve regeneration. Topography has been defined as the arrangement of the three-dimensional and structural features of a material [63, 64].

2.4.1 Cell Behavior due to Substrate Topography

The initial studies on substrate topography included the culture of embryonic neurons in grooves and filaments formed with clotting blood or fish scales [63, 65]. Even though useful, those studies did not draw clear conclusions due to the close relationship between the topographical features and chemical features of the techniques used. It wasn't until micro and nanofabrication techniques were developed that those two components were differentiated [66, 20]. Some of these new micro and nanofabrication techniques are described below. Photolithography is the formation of a pattern using a light-sensitive polymer. Ultrashort pulsed laser ablation is the use of high-intensity laser at short timescales to produce different shapes onto the material. LIGA is a hybrid technique that involves lithography, electroplating, and molding. E-beam lithography is a computer-controlled electron gun that shapes an electron sensitive material. Replica molding is the use of casting and curing 3D structures onto an elastomer, usually polydimethylsiloxane (PDMS). Electrospinning is a technique were fibers are electrostatically spun onto a scaffold. Etching uses physical and chemical means to remove parts of a material forming topographical features.

2.4.2 Substrate topography classification

There is a large range of techniques that forms different topographies onto substrates. Materials can be classified between random surface patterns and deterministic topographies. Moreover, deterministic topographies can be further classified as continuous and discontinuous. Continuous topographies consist of grooves and fibers. They can be divided into anisotropic or isotropic depending on wheatear or not those structures are directionally dependent or not. Discontinuous topographies consist of pillars and cones and can also be classified as anisotropic or isotropic. Furthermore, discontinuous topographies can also be periodic or random. Both

continuous and discontinuous substrates can be secondary classified as graded or continuous [20]. Random surface patterns are classified using roughness parameters and porosity [67].

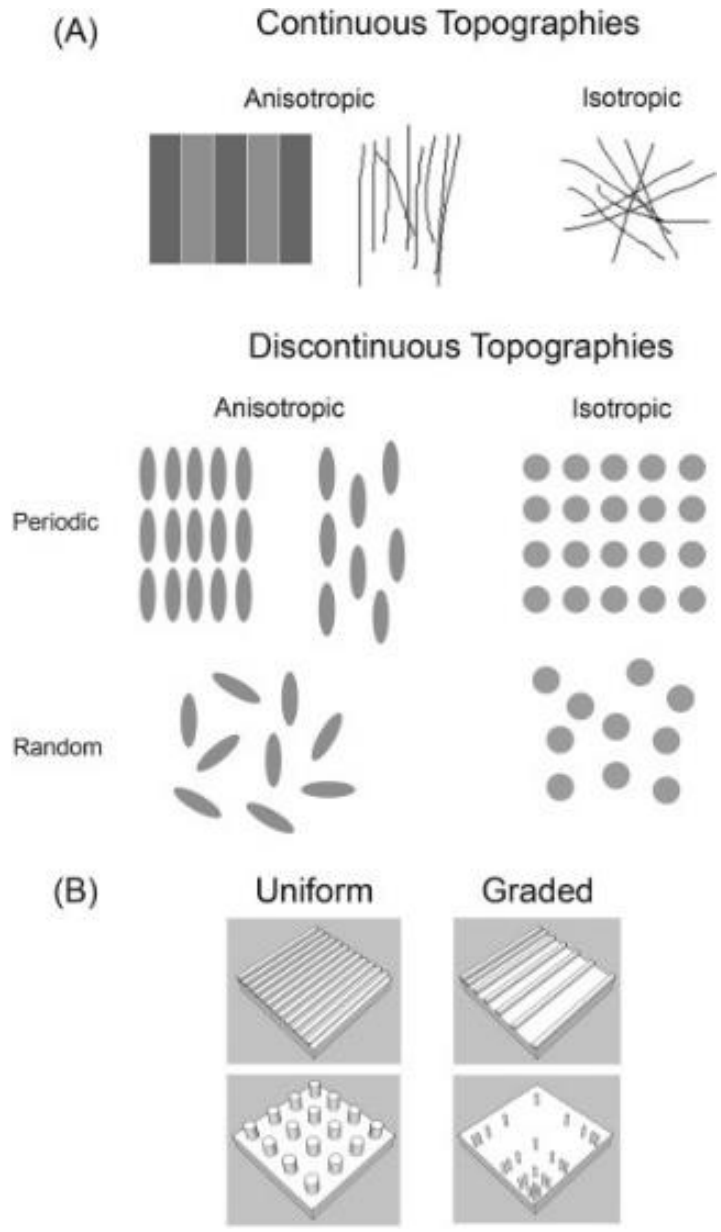

Figure 5: Classification of surface topographies. (a) Continuous and discontinuous can be both be classified as anisotropic and isotropic topographies. Moreover, discontinuous topographies can also be classified as random or periodic. (b) Examples of uniform and graded topographies within continuous and discontinuous topographies. **[20]**

2.4.3 Analysis of Surface Topography

According to the American National Standard, topography is defined as the "three-dimensional representation of geometric surface irregularities" [68]. Moreover, lay, waviness, and surface roughness are three characteristics used to define surface topography [69]. Lay refers to the overall direction of the surface configuration. Both waviness and surface roughness refers to the surface irregularities, with waviness referring to larger irregularities and surface roughness refers to fine deviations of the surface [69]. There are multiple amplitude parameters used to measure surface roughness, such as root mean square (Sq), skewness of topography (Ssk), kurtosis of topography (Sku), maximum surface peak height (Sp), maximum pit height (Sv), etc. The arithmetic mean of the absolute height (Sa) was chosen to measure the surface roughness of the aerogel samples used in this study since it's the most common parameter [70]. Sa can be described as;

$$Sa = \frac{1}{A}\int_A |z(x,y)|dxdy \tag{2.7}$$

According to the ASME B46.1 standard, there is a vast majority of instrumental techniques used to quantify surface roughness. These techniques can be classified into profiling, area profiling, and area averaging [71]. Profiling techniques provide quantitative measurements of surface peaks and valleys using a high-resolution probe. This analysis can be represented mathematically as a height function with lateral displacement, z(x) [72]. Examples of such techniques include stylus instruments, phase-shifting interferometry, and optical differential profiling. Area profiling techniques produce 3D representations of the surface roughness by scanning multiple steps forming multiple parallel profiles and can be mathematically represented as z(x,y). This technique provides more details than profiling techniques, but it is time and computer memory consuming. Some examples include atomic force microscopy, confocal

microscopy, and interferometry. Area-averaging techniques don't require as much time and CPU memory but do not provide the kind of high magnification that the other two technologies do. For this work, the technique used to measure surface roughness is white light interferometry, which is an area profiling technique.

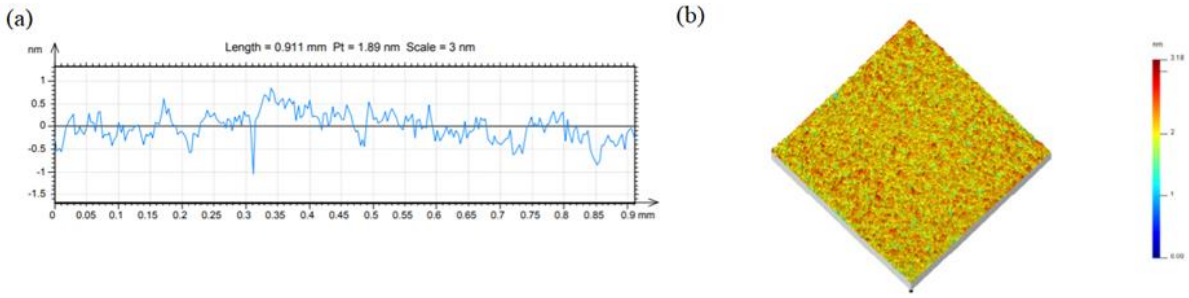

Figure 6: Types of substrate topography measurements (a) Profile measurement (b) Area measurement **[70]**.

2.4.4 White-light interferometry

An interferometer uses electromagnetic waves and the superposition of those to create an interference pattern to then extract information. When two waves are in the same phase, they show constructive interference where their amplitudes add up. On the other hand, when two waves are out of phase, they show destructive interference where the amplitudes cancel each other [72].

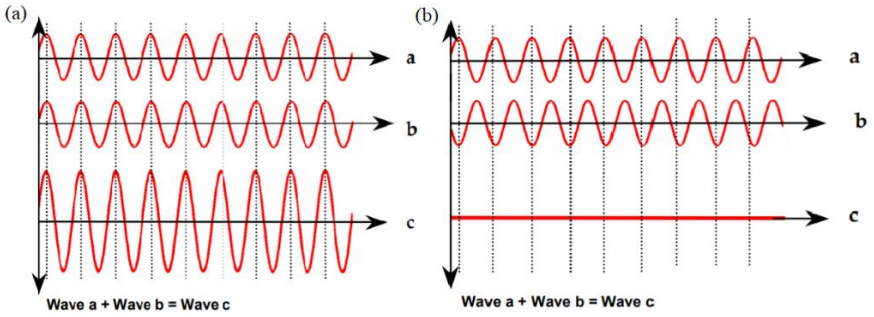

Figure 7: Interference between two waves (a) Constructive interference, wave a and b constructively interfere forming wave c. (b) Destructive interference, wave a and b destructively interfere to form wave c **[70]**.

Typically, an interferometer uses a beam of light is split into two beams and recombining them to create an interference pattern. This pattern can then be analyzed to measure the

difference in paths between the two beams. The optical path difference between them allows measuring the different heights in the sample [73], and can be described by:

$$PD = d \sin \theta \tag{2.8}$$

Were the angle θ represents the angle between the two traveling waves.

When using a white light source, beams at different wavelengths interfere, and sets of fringes for the different wavelengths are created [74].

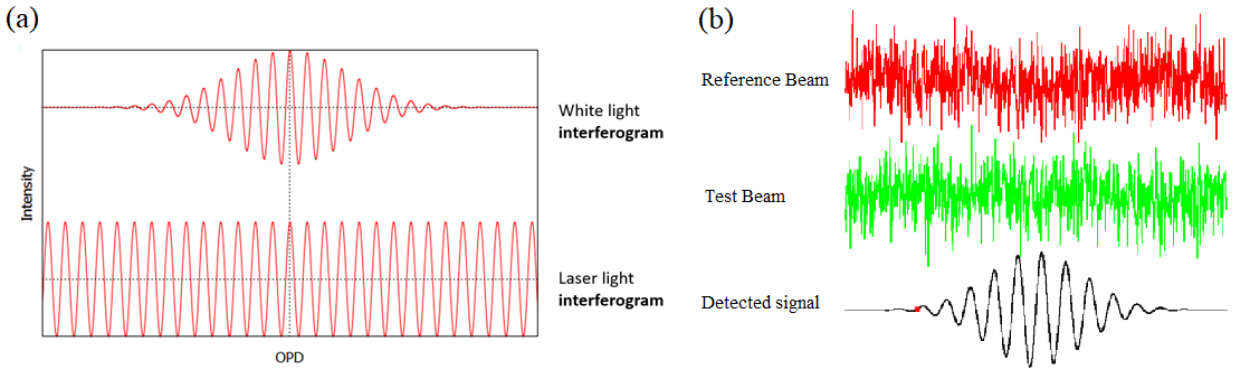

Figure 8: White light interferometry. (a) Interferogram using white light (top) vs. laser (bottom). (b) Signal from the reference beam, test beam, and the combination of both resulting in the detected signal **[75]**.

3D microscopes based on WLI use an interferometer and a computer-based scan that combines all the different wavelengths fringes into a surface roughness measurement. The results are shown as a 3D substrate with a color-coded height scale. This technique allows for fast non-contact high-resolution measurements of surface roughness [76].

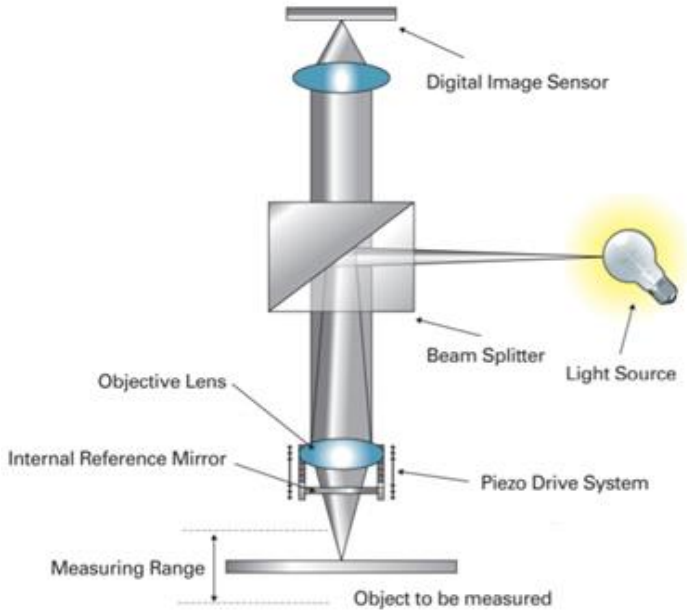

Figure 9: Set-up of a white light interferometer. Essential components of a white light interferometer consisting of the light source, beam splitter, objectives, mirrors, etc. **[70]**.

2.5 Young's modulus

Young's modulus (E) measures the material's stiffness. Mathematically, E is the ratio of stress vs. strain. Stress is defined as the force per unit area while strain is the ratio of deformation over initial length.

$$E = \frac{stress\ (\sigma)}{strain\ (\varepsilon)}\ \left[\frac{N}{m^2}\right] \tag{2.9}$$

Where,

$$stress\ (\sigma) = \frac{Force\ (F)}{Area\ (A)}\ \left[\frac{N}{m^2}\right] \tag{2.10}$$

$$strain\ (\varepsilon) = \frac{elongation\ or\ compression\ (dL)}{Lenght\ of\ object\ (L)}\ \left[\frac{m}{m}\right] \tag{2.11}$$

There are three different kinds of stress, depending on how the material is deformed. Tensile stress is used when the sample is stretched or lengthened. Compressible stress is used when the sample is compressed or shorten. Finally, shearing stress refers to a deformation with a

right-angle compared to the previous techniques [77]. The slope of the linear portion of a stress vs. strain graph represents the Young's modulus.

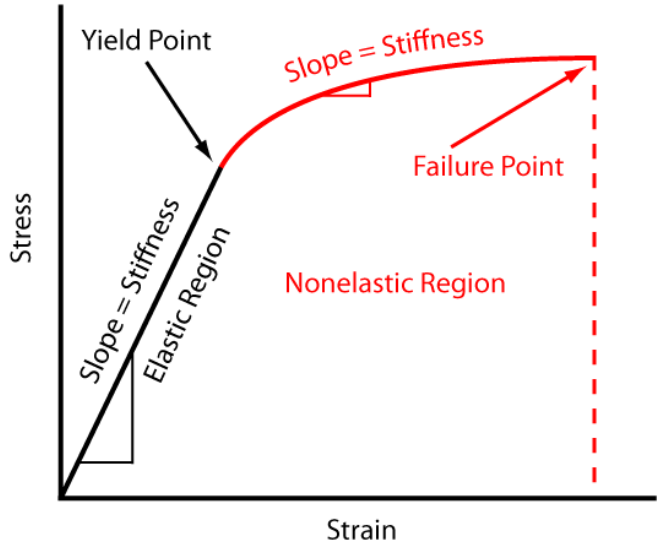

Figure 10: Graphical representation of Young's modulus. Stress vs. strain graph. The linear part (black) of the diagram represents the elastic region with its slope representing the Young's modulus. The non-linear part (red) of the chart shows the nonelastic area **[77].**

2.5.1 Cell behavior due to Stiffness

Stiffness has already been proven an essential feature of the activity and fate of cells such as fibroblasts, myocytes, smooth muscle cells, and bone marrow-derived mesenchymal stem cells [78, 79, 80]. Recent works show that Young's modulus affects stem cell differentiation [81]. Solid tissues in the body have a variety of stiffness, forming a microenvironment specific for each type of cell. Native brain tissue is a soft tissue with Young's modulus value of 0.5-1kPa, skeletal muscle is around 10kPa, cartilage, and bone have a higher order of stiffness [82, 83].

2.5.2 Analysis of Young's modulus

Stiffness with soft gels can be measured using rheology [83]. In this work, the substrates were solid, so a typical tension test was used. Often, to compare the strength of various materials, a tension test is used, where a "dog-bone-shaped" sample, is subjected to increasing tensile load [84]. The increasing load and change in length are measured during the test, and the circular

cross-section, as well as the length of the specimen, are measured previously to get the stress and strain measurements [85].

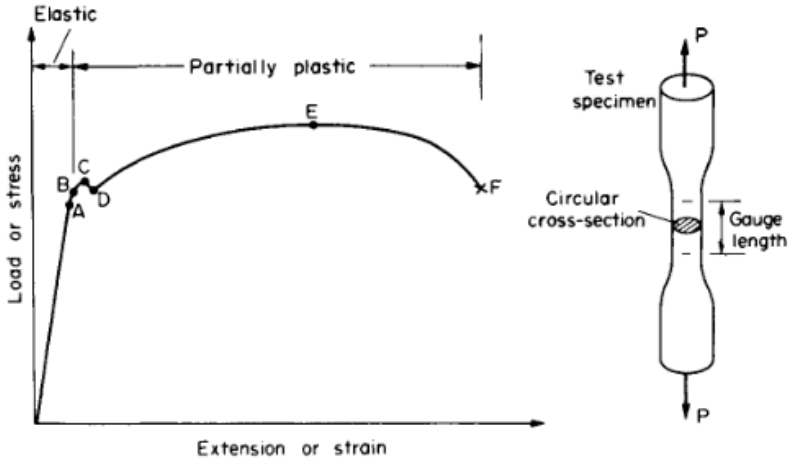

Figure 11: Diagram and example of a sample for tensile testing. Dog bone shape sample. The forces applied to the sample while experiencing tensile strain with the diagram of load vs. extension **[85].**

In this study, compression of the samples was used to measure Young's modulus. In compression testing, the stress and strain equations are the same as for tensile testing, except the force is taken negative, and the initial length is larger than the displacement. Therefore, negative stress and strain are obtained [86].

2.6 External Stimuli – electrical stimulation (ES)

Besides biochemical cues and material's properties, external stimuli are also a factor that can affect cell behavior. Due to the electrical nature of the nervous system, electrical stimulation (ES) has been used for nerve regeneration. The exact mechanism by which ES enhances nerve regenerations is not well understood. However, numerous studies show the positive effects of ES in nerve cells [87]. It has been hypothesized that electrical conduction may increase the overall differentiation and may up-regulate the essential proteins for neurite [88]. Moreover, ES may increase cell adhesion rate, neurite-bearing cell rate, and neurite alignment rate [52]**.** Sabri et al.

have already studied the effects of an electrical bias on non-conductive aerogels, but a similar study with conductive aerogels is in progress [32].

2.7 Plasmonic Photopatterning of Polyurea Crosslinked Silica Aerogels

This work has mainly focused on understanding cell behavior in random topographies. However, a study regarding a continuous topography on top of the aerogel has been investigated using aligning liquid crystal (LC) molecules thanks to a collaboration with Peng et al. Multiple techniques have been recently developed to accomplish the alignment of liquid crystal (LC) molecules into oriented patterns. Some of those techniques include: beam steering [89, 90], q-plates [91, 92], geometric phase wave plates [93, 94], programmable origamis [95, 96], controlled placement and assembly of particles [97], predesigned microfluidic electrokinetic flows in LCs, and command of active matter [98]. Recently, an approached for surface photo-patterning was published based on plasmonic photomasks and photo-alignment techniques to aqueous LC systems. This approach is biocompatible as it was used with cells (e.g., bacteria) and peptide amphiphiles [99, 100]. Moreover, this technique does not require surfactants and eliminates multiple steps of exposure to different polarized beams due to the use of plasmonic metamasks that control light polarization [101] rather than standard photomasks that control only the intensity of transmitted light.

This technique has been previously shown to manipulate the flow trajectory of bacterial cells. Liquid crystals allow to control the geometry of the cell motion, polarity of cell motion, and spatial distribution of cells. This technique can be used for designing dynamic biomaterials.

Chapter 3. Materials and Methods: Substrate Synthesis and Preparation

3.1 Introduction

The research work presented here investigated cellular response to different types of aerogels. The aerogels were selected based on the range of their surface roughness and their Young's modulus. Since the goal of this study is to understand the effect of substrate stiffness and surface roughness on the behavior of PC12 cells, substrates were selected so that a wide range of stiffness and pore size would be covered. This will assist with developing a comprehensive understanding of nerve response to substrate cues and how these factors affect cell behavior. The aerogels chosen for this study were Polyurea Crosslinked Silica Aerogel (PCSA), Carbon Aerogels (CA), and Memory Shape Polymer Aerogels (MSPA). The different aerogel types used have been summarized in Table 1. CA aerogels were provided by Lawrence Livermore National Laboratory (LLNL), and the MSPA aerogels were provided by the Leventis group, Department of Chemistry, Missouri University of Science and Technology.

Table 1: List of Aerogels used in this study

<table>
<tr><td colspan="2">PCSA
(Polyurea Crosslinked Silica Aerogel)</td></tr>
<tr><td rowspan="3">CA (Carbon Aerogel)</td><td>ACA
(Activated Carbon Aerogel)</td></tr>
<tr><td>BRF-CA
(Base-catalyzed Resorcinol Formaldehyde Carbon Aerogel)</td></tr>
<tr><td>ARF-CA
(Acid-catalyzed Resorcinol Formaldehyde Carbon Aerogel)</td></tr>
<tr><td rowspan="4">MSPA
(Memory Shape Polymer Aerogel)</td><td>Mix-14</td></tr>
<tr><td>Mix-18</td></tr>
<tr><td>aL-DEG</td></tr>
<tr><td>aL-TEG</td></tr>
</table>

3.1.1 Polyurea Crosslinked Silica Aerogel (PCSA) Preparation

Polyurea Crosslinked Silica Aerogel (PCSA) was prepared according to the methods described in detail previously [40] [102] [32] and summarized here. First, 8.75mL of methanol was added to 1.5mL of deionized water. To this mixture, 3.85mL tetramethyl orthosilicate (TMOS) (Sigma-Aldrich) and 0.25mL (3-aminopropyl) triethoxysilane (APTES) (Sigma-Aldrich) were added and mixed for 15 sec, which then formed a colloidal suspension. The mixture was then poured into cylindrical molds, covered in methanol (Sigma-Aldrich), and allowed to cure for 12-24 hrs. The gels were in a 4-day acetonitrile bath with washes repeated every 24 hrs. To cross-link the gels, they were placed in a 33gr Desmodur N3200 (Bayer) and 94mL acetonitrile (Sigma Aldrich) mixture for 24 hrs placed in an acetonitrile bath in a 70˚C oven for 3 days and washed every 24hr with acetonitrile for 4 days. The gels were then dried in a critical point dryer (CPD) and stored in an environmental chamber until needed.

3.1.2 Carbon Aerogel (CA)

Carbon aerogels (CA) combine the unique 3-D aerogel topography with electrical conductivity, thermal and chemical robustness, and excellent mechanical properties not observed in other aerogel materials [103, 104]. The inherent electrical conductivity of CA, combined with the 3-D surface and 3-D printed capabilities, makes them an attractive candidate for biomedical applications [105].

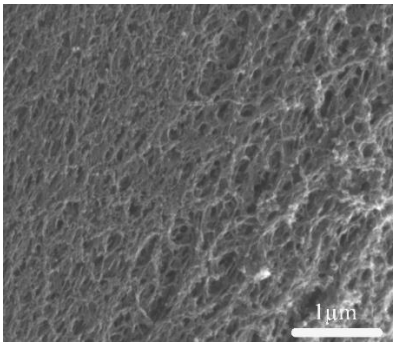

Figure 12: SEM image of CA structure. SEM image of the nanoporosity of BRF-CA.

Three different types of carbon aerogels were used in this study. Acid-catalyzed resorcinol formaldehyde (ARF-CA) carbon aerogel and base-catalyzed resorcinol formaldehyde (BRF-CA) carbon aerogels and Activated Carbon Aerogel (ACA) which have very different pore structure and pore diameters. ARF-CA has a pore diameter typically larger than 1µm while BRF-CA has pores typically less than 1µm. Both ARF-CA and BRF-CA follow a similar method for synthesis. Resorcinol and formaldehyde were mixed with water and acetic acid, with different proportions of those chemicals for each type. Those gels were cured and then soaked in acetone followed by supercritical drying in liquid CO_2 at a critical temperature of 55°C and at a pressure range of 1200-1400 psi. The aerogels were subjected to a heat treatment process where the samples were heated in a tube furnace under a nitrogen atmosphere at 1050°C for 3hrs with a heating and cooling rate of 2°C/min. BRF-CA and ARF-CA samples were sterilized as previously described [106, 88]. Figure 13 shows the basic outline for CA synthesis.

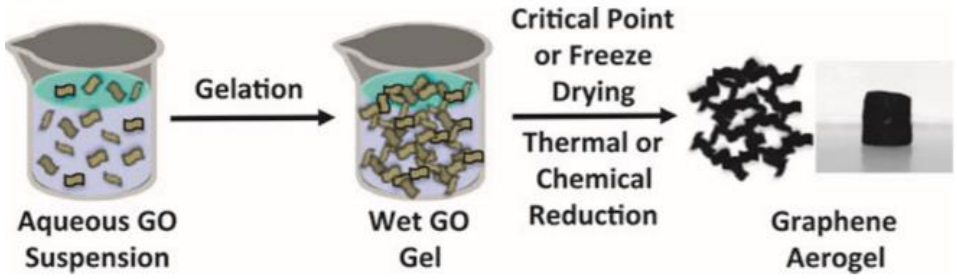

Figure 13: Diagram of CA Synthesis. Sol-gel synthesis of graphene-based aerogels with the main steps represented; gelation, CPD, and end result **[105].**

3.1.3 Shape Memory Polymer Aerogel (SMPA)

Shape Memory Polymer Aerogels (SMPA) are soft flexible aerogels that differ greatly from their silica and carbon-based counterparts. It is a new class of aerogels that combines the low density and high porosity expected of aerogels with the features of shape-memory materials (SMMS), which undergo deformation and recovery. An external stimulus such as temperature triggers a shape memory effect in these materials. A triisocyanate core accomplishes this effect

with rigid isocyanurate cross-linking nodes that allow the aerogel to restore its shape after deformation. This memory shape effect is explained by the strain of the Mixed-Alcohol poly(isocyanurate-urethane) (PIR-RUP) aerogels above glass-transition temperatures (T_g) followed by fixing them in the temporary shape at temperatures below T_g and reheating them back to high T_g temperatures. Four different types of SMPAs were investigated in this study. The differences between them reside in the proportions of the precursors as well as the gelation time [107] which in turn lead to differences in pore size and the elastic modulus. Figure 14 shows the reagents and chemical reaction for SMPA synthesis.

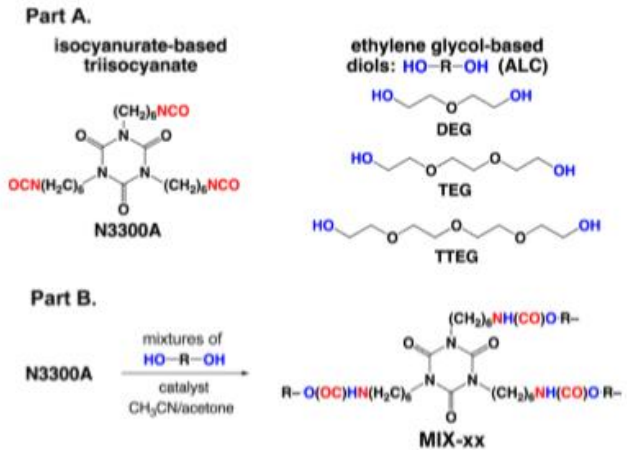

Figure 14: Diagram of SMPA synthesis. (a) Reagents for synthesis of SMPA. (b) Chemical reaction for SMPA. **[107]**.

3.2 Aerogel Characterization

The material properties of the aerogels presented so far were characterized to further investigate the relationship between the cell behavior and the material's properties (surface roughness and Young's modulus).

3.2.1 Surface roughness

High-resolution 3D images of the substrates and cells were obtained using the Profilm3D (Filmetrics Inc. San Diego, CA) profilometer. Prepared samples were sputter-coated prior to imaging. Image analysis was performed using the web-based software from Filmetrics. The area

roughness analysis was determined using the arithmetic mean height (Sa) over an area of 200x200μm^2. Three independent trials (n=3) were performed. Each trial consisted of ten separate measurements (N=10).

3.2.2 Young's modulus measurements

The compressive test was performed using the ESM303 motorized test stand, and the Series 5 digital Force Gauge (Mark-10 Corp, Copiague, NY). The extension rod G1024 and a compression plate G1009 were attached to the 100N gauge to perform the compression studies. The system was set to perform all experiments at a compression rate of 0.5mm/min to measure the load (N) versus the traveled distance (mm). The compressive strength of all substrates used in this study were measured both under dry conditions as well as while submerged in cell culture medium for 24 hrs at 37°C to simulate cell culture conditions. Results have been reported in the next chapter.

Chapter 4. Materials and Methods: Neuronal Cell Culture

4.1 PC12 cells

PC12 cells have been extensively used as a model for peripheral neurons due to their response to nerve growth factor (NGF) with the outgrowth of axon-like neurites [108] and their expression of neuronal markers such as peripherin [109]. Peripherin is a neuronal intermediate filament protein mostly found in the peripheral neurons. This protein helps assemble filamentous network forming unique molecular shapes [110]. Moreover, PC12 cells have been extensively used as a model to explore the influence of electrical stimulation [111, 112, 32].

4.2 PC12 cells culture conditions

PC12 pheochromocytoma cells obtained from the American Type Culture Collection (ATCC, Manassas, VA) were grown in RPMI 1640 medium supplemented with GlutaMax, HEPES buffer (Life Technologies, CA), complemented with 10% heat-inactivated horse serum, 50 µg/mL penicillin/streptomycin, and 5% fetal bovine serum, forming a complete medium [25]. Cells were seeded at a density of $1x10^4$ cells/cm^2 in all cases. Cells were sustained in a 5% CO_2 incubator at 37°C. Three independent trials (n=3) were prepared for each experiment, and a control (TCPS) was run in parallel for each trial. Results were averaged over three separate trials for each set of conditions.

4.3 Priming of PC12 cells

Before each experiment, PC 12 cells plated on collagen I coated TCPS cells were "primed" for neural differentiation. Priming of cells consisted of culturing cells with 50 ng/ml NGF for 8 days an RPMI 1640 medium supplemented with GlutaMax, HEPES buffer, 1% horse serum, and penicillin/streptomycin. This medium was replaced every 2-3 days. After 8 days, the cells were collected from the dish, centrifugated at 550rpm, cell clusters were broken by passing

them through a 22g needle, and frozen until used for experiments. Details of this protocol have been described previously [113].

4.4 Collagen Coating

Aerogels and TCPS substrates were washed in ethanol and sterilized for 30 min under ultra-violet (UV) light (254nm). The substrates were then coated with collagen. Rat tail type 1 collagen (Invitrogen, Carlsbad, CA) was diluted to a concentration of 0.05 mg/ml in 20 mM acetic acid [32, 102]. The collagen solution was laid on the substrate to reach a protein density of 4 $\mu g/cm^2$ and allowed to sit for 1 hr at room temperature and under sterilized conditions. The excess collagen solution was then removed with a vacuum line, and the samples were rinsed twice with serum-free RPMI 1640 prior to the cell culture step [32, 42]. This protocol was modified when culturing PC12 cells onto SMPA. The ethanol step was replaced by using a serum-free medium. This change was caused by an increase in volume observed when submerged in ethanol. It has been hypothesized that the expansion was still occurring during cell culture. However, an improvement was found when the ethanol step was substituted for a serum-free medium. Even though this modification showed a higher density of cells attached, the overall number of cells observed was lower than previous substrates.

4.5 Fixation for Scanning Electron Microscopy

Samples were fixed in 2.5% glutaraldehyde (Tousimis, Rockville, MD) in 0.1M sodium cacodylate buffer for 15 min, drop by drop. The medium-glutaraldehyde mixture in the substrates was substituted with 2.5% glutaraldehyde in 0.1 sodium cacodylate buffer for 2 hrs at room temperature. Following this bath, two times 10 min washes with 0.1 M sodium cacodylate buffer were performed. Samples were immersed in an aqueous solution of 1% osmium tetroxide (Electron Microscopy Sciences, Hatfield, Pa) for 1 hr at low temperature. After this immersion, two washes

of 10 min in sodium cacodylate buffer were performed, and then the samples were dehydrated by a series of 10 min each washes in 10%, 30%, 50%, 70%, 90%, and 100% ethanol. Finally, all substrates were fully air dry before sputter deposition of 10 nm gold/palladium film before imaging [32, 42].

4.6 Scanning Electron Microscopy

Nova NanoSEM 650 Field Emission Scanning Electron Microscope (FEI, Hillsboro, OR, USA) or a Phenom Pure Desktop SEM (PhenomWorld, Nederlands) were used to image the samples. The FEI Nano NanoSEM 650 ESEM scanning electron microscope was equipped with a through lens detector (TLD) in secondary electron (SE) operation. The imaging was carried out in field-free lens mode at the primary electron energy of 30 keV. The working distance was adjusted to 5 mm. The Phenom Pure desktop Scanning Electron Microscope (SEM) was operated using the 10keV and Backscatter electron detector (BSD) in full mode [32, 42].

4.7 Analysis of the Cell Properties

Five different cell properties were measured to understand the impact of the different substrates and their unique properties on the PC12 cells. These were contact area, neurite length, number of neurites per cell, number of branches per neurite, and length of branches, as described in Table 2. These properties were measured using NIH open-source software Image J. The overlaid scale bar from the SEM images was used to calibrate the measurement tools and therefore allowing for accurate measurement of those morphological parameters. Figure 15 shows a representative SEM image where the traces were created using ImageJ and superimposed on a PC12 cell to measure the different cell properties. In blue, the perimeter of the cell area was estimated to get the contact ell area. In green, the neurites were traced to show how they were measured. The

amount of neurite traces per cell body was used to measure neurite density. A similar process was followed for neurite branches and is shown in yellow.

Table 2: Description of all cell properties measured in this study.

Cell Properties	Unit	Definition
Neurite length	µm	The longest cytoplasmic extensions that originate from the cell body.
Neurite density		The Amount of neurite traces per cell body.
Contact area	μm^2	Area surrounded
Branch length	µm	Cytoplasmic extension originating from another extension
Branch density		Number of branches per neurites

Neurite selection was performed as defined in detail elsewhere [32, 40]. Neurites were treated as vectors and measured with a series of straight-line segments using the line segment tool. Neurites were defined as the most extended cytoplasmic extensions originating from the cell body and were also counted per cell body. The cell body perimeter was underlined to get its contact area using the freehand tool, which allowed to create irregular shapes following the cell perimeter. Branches originating from neurites were counted and measured using the same method as neurites.

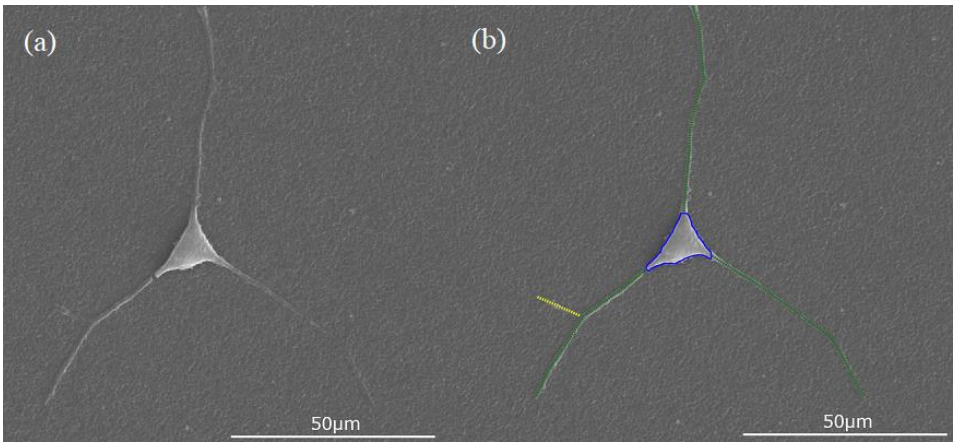

Figure 15: Traces of the cell properties using SEM images and ImageJ. (a) Original SEM image (b) SEM image with superimposed traces. In blue, the contact cell area is shown. The neurite length trace is shown in green. The branch length is shown in yellow.

In some of the studies presented here, the neurite orientation is also essential to evaluate. In that case, the cell body was treated as the origin point of a polar plot (Figure 17b), and the neurite orientation was measured with an angle from 0° to 360° using the straight-line tool (Figure 17c). For the substrate with a linear plasmonic photo-pattern, the analysis was carried with the pattern in the orientation of the 0° and 180°, while studies with an electrical the cathode was orientated on the north pole. The overall direction of the neurites was determined using the following vector projection analysis:

$$x = \frac{1}{N}\sum_{i=1}^{N} L_i \cos\theta_i \quad \textbf{(}4.1\textbf{)}$$

$$y = \frac{1}{N}\sum_{i=1}^{N} L_i \sin\theta_i \quad (4.2)$$

where N is the total number of neurites measured, L is the individual neurite length, and θ represents the neurite angle from the horizontal axis [11].

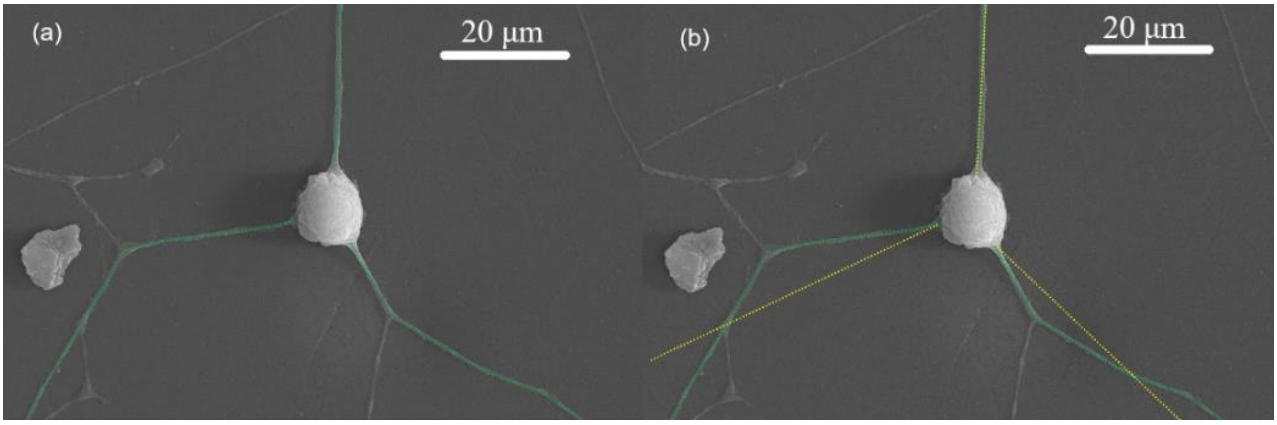

Figure 16: Measurement of neurite alignment. (a) Neurite length is measured using ImageJ, as previously described. (b) The straight-line tool was used to measure the angle of the neurite by lining it with the overall orientation of the neurite.

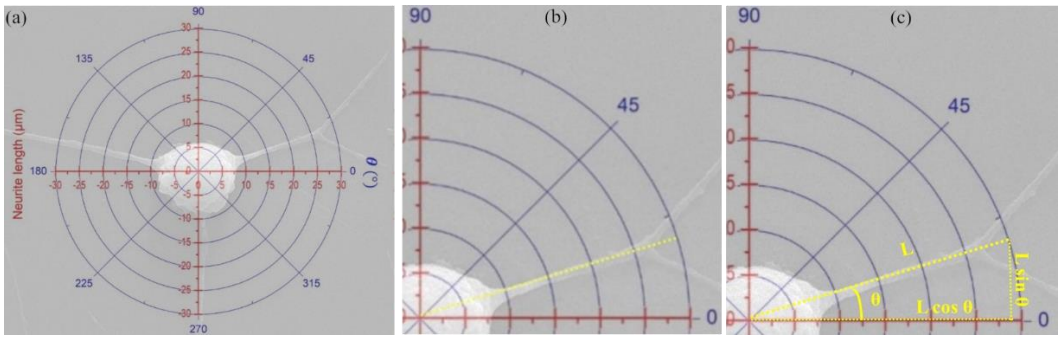

Figure 17: Measurement of the angle of the neurite. (a) The cell body is used for the origin of the polar plot. (b) The neurite alignment is used as the basis to measure the angle of the neurite. (c) Polar plot representation of the neurite measured.

4.8 Collagen Characteristics

To attach and grow PC12 cells on aerogels and TCPS, a layer of collagen was first placed. To better understand the effect of the aerogel substrate on the PC12 cells, it was important to first understand how the aerogels affected the behavior of the collagen layer, if at all. The different substrates were prepared for cell culture as described previously, with sterilization as well as collagen coating, after which the samples were fixed, and sputter coated. Topographical analysis of the collagen-coated substrates was compared with the topographical analysis of the substrates without any collagen coating. SEM images of the collagen-coated substrate were observed and analyzed to fully understand the differences between the substrates [32, 42].

4.9 Statistical Analysis

Statistical analysis to determine differences between experiments were performed using a two-tailed student's t-test. The student's t-test is used to compare the averages of two samples to see if there is a significant difference between them [114]. A p-value or probability value is calculated to determine the significant difference between the two sets. The average of both sets was determined to be significantly different if the p-value is smaller than 0.05 ($p < 0.05$). Neurite length, cell area, neurites per cell, and neurite branches were calculated in different substrates in

three independent trials. Each trial consisted of 100 to 200 measurements. The average of those measurements was used for the standard deviation. The error bars used in graphs were obtained by calculating the standard error of mean using the three independent trials (n=3) performed. Statistical analysis and error bars were determined using Excel 2016. Graphs were obtained using Origin9.

4.10 Electrical Stimulation

As published previously [32], an electrostimulation device was used to provide a DC bias, while PC12 cells were cultured onto the ARF-CA to understand how a conductive substrate would affect the cell behavior. Electrodes used in this study were constructed as previously described [32] . ARF-CA and TCPS substrates were first coated with four µg/cm2 collagen (Invitrogen), as discussed previously and seeded with primed PC12 cells (Figure 18).

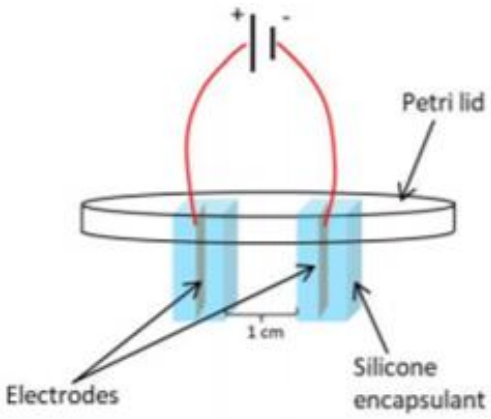

Figure 18: Electrical stimulation chamber: (a) Schematic diagram of the custom-built electrical stimulation chamber used for ARF-CA and TCPS substrates **[32]**.

4.11 Plasmonic Photo-Patterning

It has been previously shown the importance and impact of continuous topographies on cell behavior. Cells cultured onto continuous topographies extend longer neurites with directionality. A precise patterning of aerogels and glass (control) was created using a plasmonic

photo-patterning technique. The photosensitive azodye material SD1 (Sigma-Aldrich, St. Louis, MO) and n,n-dimethylformamide solvent at 0.3 wt% concentration were mixed. This solution was spin-coated on cleaned aerogel discs at 3000 rpm for 30 sec. The aerogel disks were heated at 90°C for 30 min and then exposed for 5 min in the photo-patterning exposure system with photonic meta-mask [98]. The custom-made photonic masks made of aluminum film contained the desired pattern with a 150nm thickness, perforated with rectangular nanoslits, each of a length 220nm and width 100nm. The photosensitive substrate was irradiated through the photomask with a predesigned pattern. The irradiation causes the locally polarized beam to realign the photosensitive molecules of SD1 perpendicularly to the polarization of light. Therefore, the polarization pattern of light was imprinted onto the photosensitive layer that was used to align the liquid crystal.

SD1 is a partly water-soluble compound. An additional layer of polymerizable material was added, causing a separation of the SD1 layer from the water. A mixture of monomer RM257 (EM Industry) and toluene at the concentration of 10 wt% with photoinitiator Irgacure 651 (Ciba, Inc, Base, Switzerland) at the concentration 5 wt% of RM257 was prepared. This solution was spin-coated onto the SD1 aerogel disks at 3000 rpm for 30s and then heated at 55°C for 5 min to evaporate the solvent and photo-polymerize under an unpolarized ultraviolet (UV) light with an intensity of 1.4 mW/cm2 for 30 min. This liquid crystalline polymer pattern was expected to replicate the pattern of SD1 alignment beneath it. Aerogel disks and glass slides containing the pattern were then ready for cell culture. Preparation of plasmonic photo-patterning onto substrates courtesy of Dr. Chenhui Peng [115].

Chapter 5. Results and Discussion: Response of PC12 Cells to Substrate Properties

5.1 Viability of PC12 Cells on Aerogels

In this section, the results of culturing PC12 cells on 5 different types of aerogels are reviewed and the focus will be on viability and success or failure of the methodology. These aerogels were listed in Table 1 (Chapter 3) following sections describe the results of growing PC12 cells on different aerogel substrates and any complications associated with working with each type of aerogel. The methods described in Chapter 4 were used as the baseline for PC12 cell culture.

5.1.1 Polyurea Crosslinked Silica Aerogels (PCSA) as a Neuronal Scaffold

PCSA has been successfully used as a substrate for PC12 cell differentiation and neurite outgrowth, which has been observed routinely and repeatedly. An example is shown in Figure 19 where both SEM and profilometry images capture the outline of a cell cluster containing extensions on this aerogel substrate.

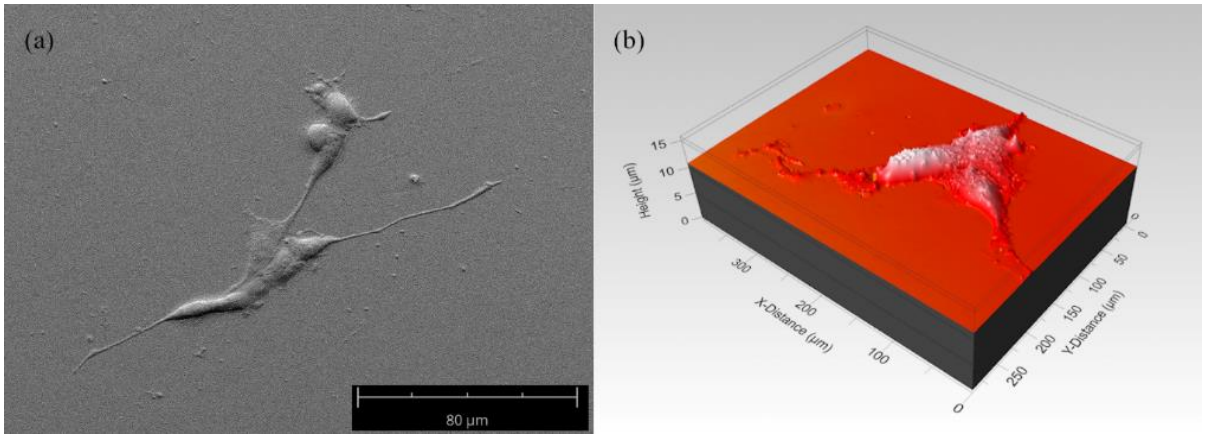

Figure 19: PC12 cell culture onto PCSA. PC12 cells were successfully attached and differentiated in PCSA. (a) SEM image of cells cultured on PCSA. (b) Profilometer image of cells cultured on PCSA.

5.1.2 Activated Carbon Aerogel (ACA) as a Neuronal Scaffold

Activated Carbon Aerogel was successfully used as a substrate for PC12 cell attachment and differentiation. However, ACA is inherently more brittle than other types of aerogels and the processing steps required for fixing cells made this substrate challenging to work with. While cell proliferation and neurite extension were observed, large fissures appeared in the aerogel structure and as a result it was not possible to reliably measure cell properties.

5.1.3 Based-catalyzed Resorcinol Formaldehyde Carbon Aerogel (BRF-CA) as a Neuronal Scaffold

BRF-CA was successfully used as a substrate for PC12 cell differentiation (Figure 20). The methods described previously were followed without any obstacle, resulting in cell attachment and differentiation that were analyzed and discussed in a future section. No deformities or fissures were observed.

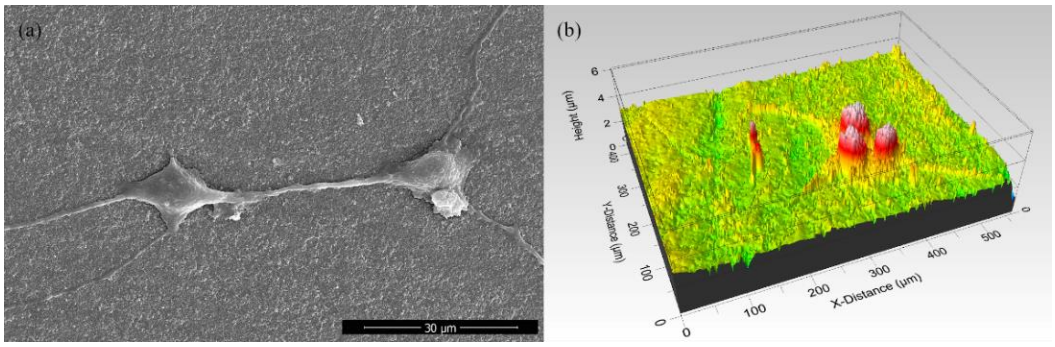

Figure 20: BRF-CA as a substrate for cell culture. PC12 cells were successfully attached and differentiated in BRF-CA. (a) SEM image of cells cultured on BRF-CA. (b) Profilometer image of cells cultured on BRF-CA.

5.1.4 Acid-catalyzed resorcinol formaldehyde Carbon Aerogel (ARF-CA) as a Neuronal Scaffold

ARF-CA was successfully used as a substrate for PC12 cell attachment and differentiation. Like BRF-CA, no modifications of the baseline methods were made since the PC12 cells attached and differentiated (Figure 21).

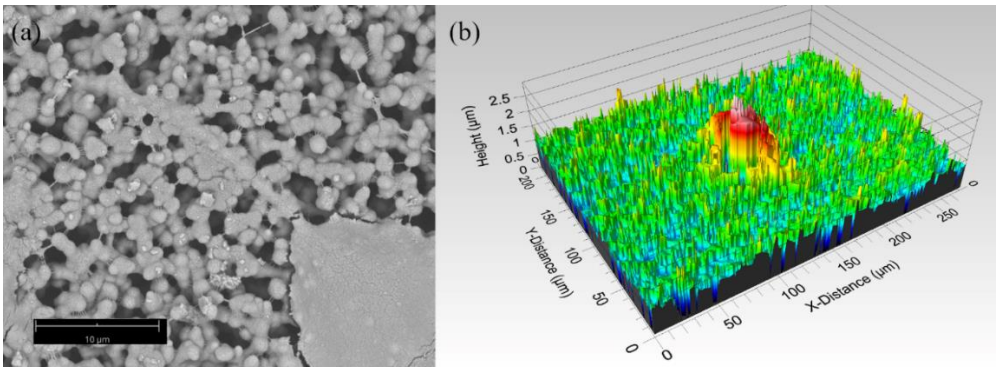

Figure 21: ARF-CA as a substrate for cell culture. PC12 cells were successfully attached and differentiated in ARF-CA. (a) SEM image of cells cultured on ARF-CA (b) Profilometer image of cells cultured on ARF-CA.

5.1.5 Shape Memory Polymer Aerogel (SMPA) as a Neuronal Scaffold

Four different SMPAs were successfully used as a substrate for PC12 cell differentiation; Mix-14, Mix-18, aL-DEG, and aL-TEG (Figure 22).

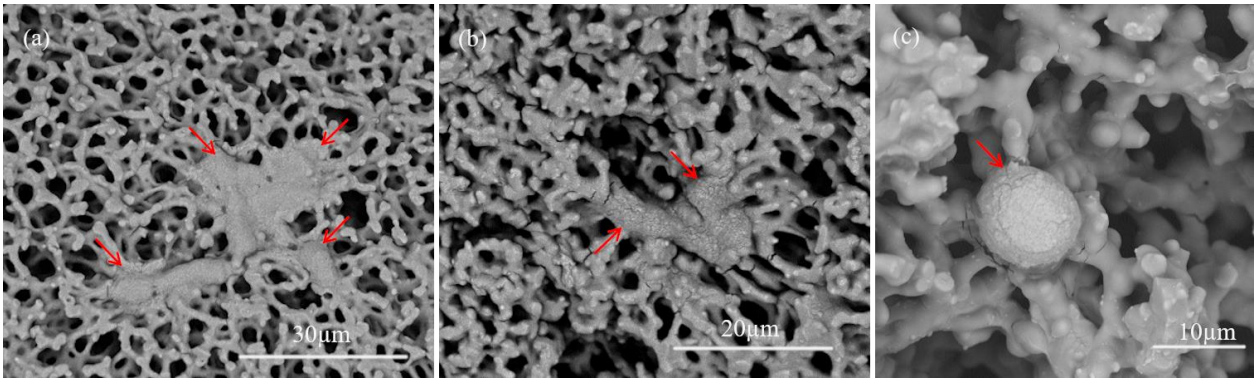

Figure 22: SMPA as a substrate for cell culture. (a) SEM image of cells cultured on Mix-14. (b) SEM image of cells cultured on Mix-18 (c) SEM images of cells cultured on aL-TEG.

5.2 Response of PC12 cells

Those aerogels that were successfully processed in the previous section were further analyzed and the response of PC12 cells was quantified. In this section the behavior of PC12 cells on each substrate type is summarized. For each substrate type, five cell properties were measured and are reported here. These are contact area, neurite length, neurite density, neurite branching, and finally branch length, as listed in Table 2 (Chapter 4).

5.2.1 Response of PC12 cells to PCSA

The contact area was measured and compared to the contact area of those cells cultured onto the control (TCPS). A smaller contact area was measured in cells cultured on PCSA. Neurite length and neurite density were measured, and the results were similar to previously published work [32] and confirmed our previous observations. Neurites were longer on PCSA than on the control (TCPS) substrates, while the neurite density was smaller when compared to the cells cultured on the control (TCPS). Both neurite branching and branch length were measured and found to be shorter with lower density when cultured on PCSA compared to the control (TCPS).

5.2.2 Response of PC12 cells to BRF-CA

A similar trend to that of cells cultured on PCSA was found in those cultured BRF-CA regarding contact area, neurite length, neurite density, branch density, and branch length. The contact area was found to be smaller when cells were cultured in BRF-CA than the control (TCPS), while neurite length was more significant. Neurite density, branch length, and branch density was also found to be smaller when cells were cultured in BRF-CA than the control (TCPS)

5.2.3 Response of PC12 cells to ARF-CA

ARF-CA was effectively used as a substrate for PC12 cell culture, and similarly, all parameters regarding cell properties were measured. The contact area was found to be smaller when cultured in ARF-CA than the control (TCPS). Similarly, neurite length was also found to be shorter when cells were cultured in ARF-CA compared to the control (TCPS). Neurite density was found to be larger in cells cultured in ARF-CA compared to the ones cultured on the control

(TCPS), while branch length and branch density was measured to be smaller when cultured in ARF-CA.

5.2.4 Response of PC12 cells to SMPA Mix-14 and Mix-18

Mix-14 and Mix-18 SMPA supported cell attachment and differentiation; however, not all cell properties were measured. Only cell area, neurite length, and neurite density were observed and analyzed. All three measurements were found to be smaller in cells cultured in SMPA Mix-14 and Mix-18 than those cells cultured on the control (TCPS).

5.2.5 Response of PC12 cells to SMPA aL-DEG and aL-TEG

In contrast to previous substrates, aL-DEG and aL-TEG SMPA showed a lower success rate for cell attachment, and no neurite extensions were observed. Like the other SMPA substrates, the methodology was slightly changed to take into consideration the volume expansion found during the sterilization step using ethanol and was exchanged for serum-free medium. A smaller amount of contact cell area measurements was made in comparison to previous substrates, and no analysis was made for the other four cell properties.

5.2.6 Summary of Response of PC12 cells to Aerogels

The cell responses reported in the preceding sections are now summarized and shown in Figure 23. Three independent trials (n=3) with a hundred measurements each (N=100) were used to create this Figure. As the graph shows, the cells cultured on the control (TCPS) were measured to have a larger contact area than the cells cultured on any of the aerogel substrates. According to the t-test, the difference between the control and all other aerogel substrates is statistically significant (*) with $p < 0.05$.

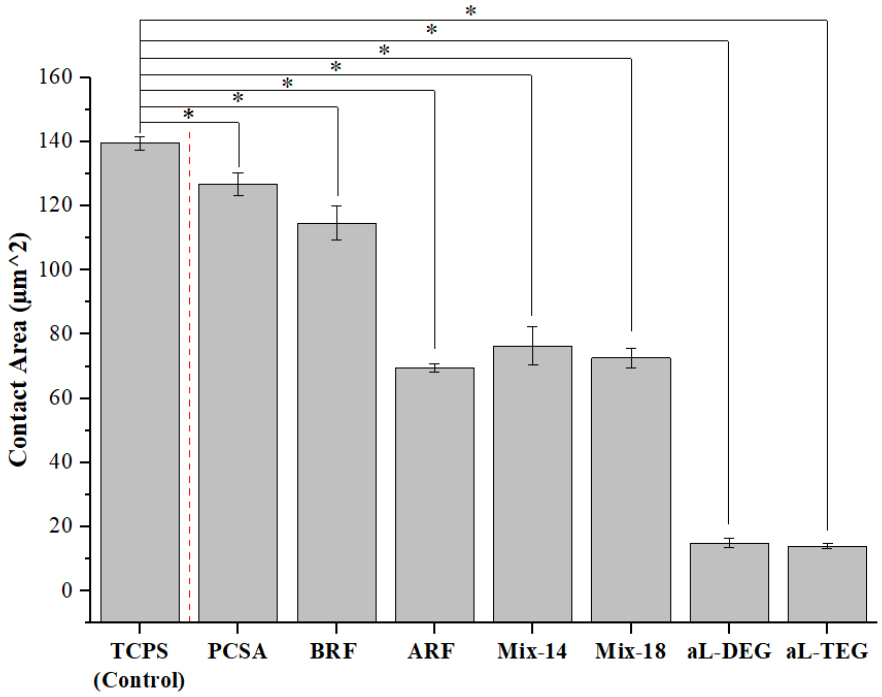

Figure 23: Contact Area averages of PC12 cells cultured on different substrates. Contact area measured on cells cultured on each substrate used in this study. Statistical significance (t-test) with $p<0.05$ (*) found between all substrates compared to the control (TCPS).

For *in vitro* experiments, neurite length is a critical parameter that helps identify the best substrate to support nerve regeneration. Figure 24 shows the average values for the neurite length measurements on all substrates discussed earlier in this chapter. The most noticeable feature is the increase in neurite length for those cells cultured on PCSA and BRF-CA aerogels when compared to the control. On the other aerogels namely ARF-CA, SMPA, the neurites measured were shorter than those on the control and on PCSA and BRF aerogels. All measurements made showed a statistically significant difference by the t-test, $p < 0.05$ (*) compared to the control (TCPS).

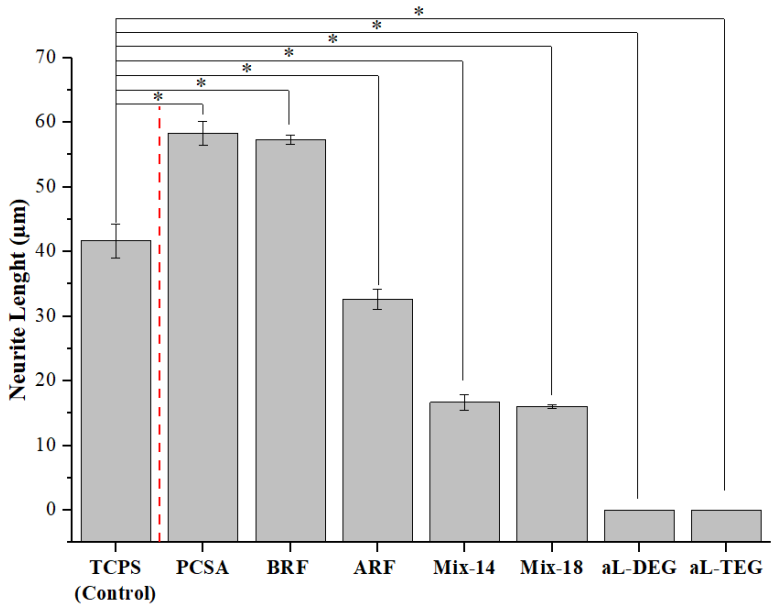

Figure 24: Neurite length averages of PC12 cells on varying substrates. Neurite length average for the cells cultured in each substrate used in this study. Statistical significance (t-test) with $p < 0.05$ (*) found between all substrates compared to the control (TCPS).

Neurite density (defined as the number of neurites per cell body) was also measured for all substrates and summarized in Figure 25. All aerogel substrates showed a lower neurite density compared to TCPS (Control) with a statistical significance according to the t-test $p<0.05$ (*).

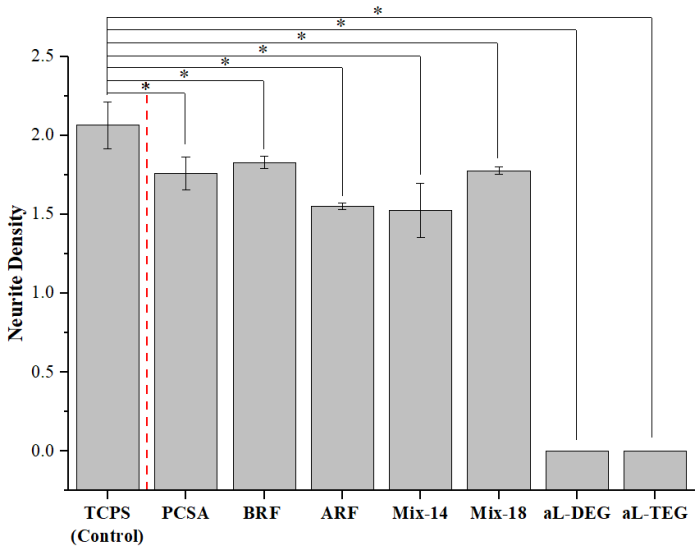

Figure 25: Neurite density averages of PC12 cells on different substrates. Neurite density average measured on the cells cultured in each of the different substrates used in this study.

Following contact cell area, neurite length, and density, the next cell property measured was branching; branch length and branch density. As previously stated, only three aerogel substrates showed branching. The averaged values of the cells with branches showed a $p < 0.05$ in the t-test compared to those cultured on the control (TCPS). Figure 26 shows the average branch length of the cells cultured on all the different substrates compared to the control (TCPS). PC12 cells cultured onto the SMPA substrates showed no neurite extensions. Consequently, no branches were observed either. Therefore, a value of zero is shown for both branch length and branch density. Within the different aerogels, the cells cultured on BRF-CA exhibited the shortest branch, while those cultured on PCSA and ARF-CA had longer branches.

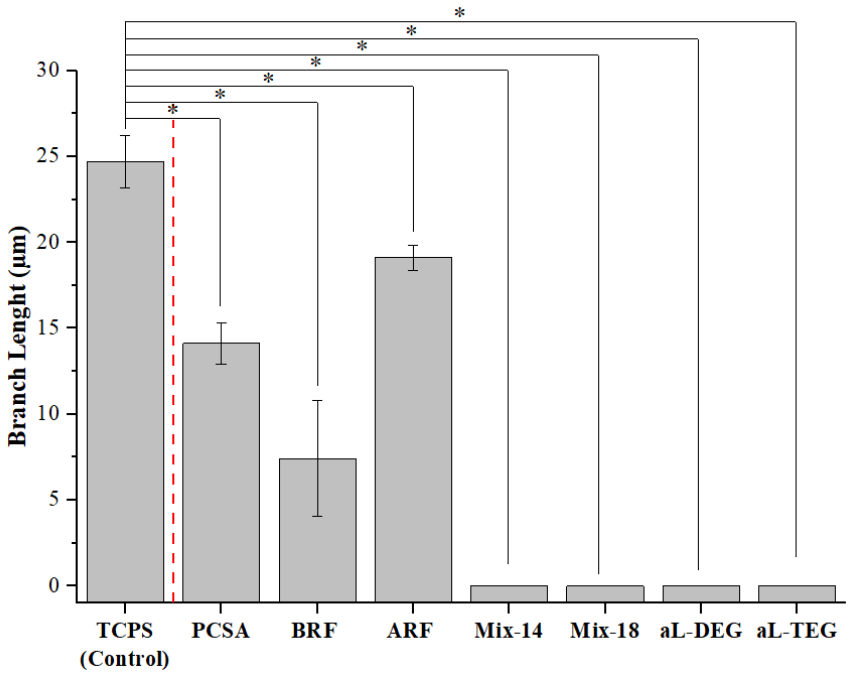

Figure 26: Branch length averages of PC12 cells on various substrates. Branch length average measured on cells cultured in each substrate used for this study. Statistical significance (t-test) with $p < 0.05$ (*) found between all substrates compared to the control (TCPS).

A similar process was performed for branch density, defined as the number of branches per neurite. Figure 27 shows the average branch density for all substrates. For the cells cultured onto SMPA substrates, no branches were observed and an expected value of zero is shown on

those substrates. A similar pattern is found in branch density as in branch length, where the cells cultured on the control (TCPS) had the highest value with a statistical difference compared to the non-SMPA aerogels.

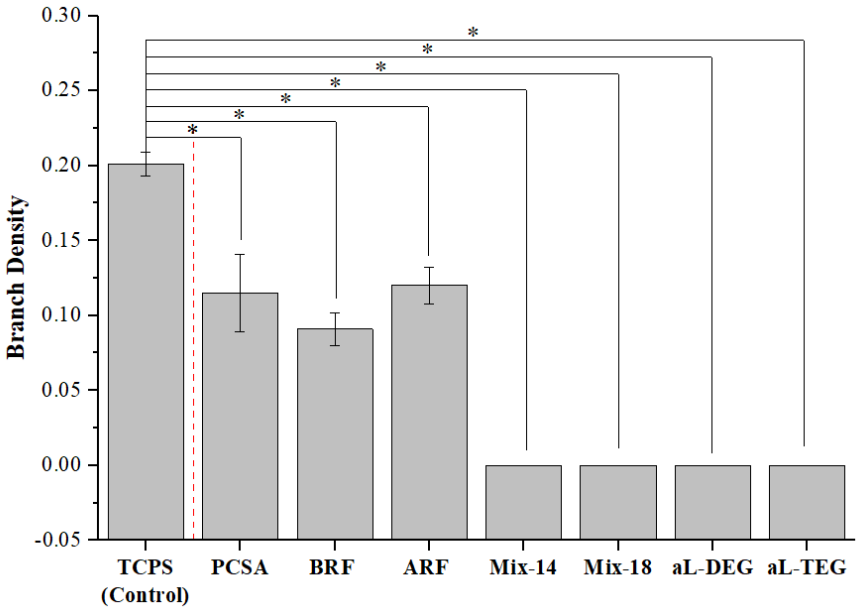

Figure 27: Branch density averages of PC12 cells on different substrates. Branch density as a function of varying aerogel and control (TCPS). Statistical significance (t-test) with $p < 0.05$ (*) found between all substrates compared to the control (TCPS).

5.3 Collagen Behavior

After observing the cell behavior of PC12 cells on different aerogel substrates, another apparent difference was observed, collagen behavior. According to the manufacture of the collagen used, the collagen should be presented as a firm, clear gel. Throughout the experiments performed in this study, two different morphologies were observed, first the morphology described by the manufacturer as a nanometer-scale thickness gel that rests between the aerogel substrate and the cells. This morphology was observed in substrates of small pore diameter in the BRF-CA (Figure 28a) and the PCSA. However, in a larger pore diameter, the collagen was mainly observed as a layer of dispersing fibers (Figure 28c). This dual morphology can be further seen in some areas of the larger pore diameter substrates. After a closer look into the

substrates with a larger pore diameter, the initial observation of change in morphology of the collagen can be further assessed. In those areas of the large pore diameter substrate where the structure of the aerogel has a larger contact area, space is created for the gel of collagen to rest. Those spaces showed a thin layer of collagen gel formed by fibers (Figure 28b).

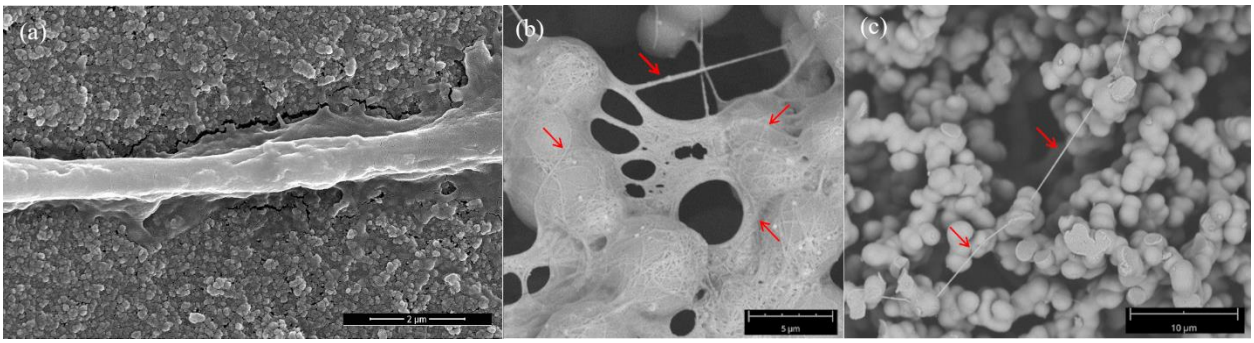

Figure 28: The three different collagen morphologies found. (a) In small nanometer pore diameter substrates, a homogeneous thickness layer is deposited on top of the substrate where the collagen fibers are not observed. (b) In micrometer pore diameter substrates that have areas with larger contact area, the layer of collagen is seen as a thin film of fibers that stretch over the substrate. (c) Collagen in the form of filaments without the formation of a thin film.

The collagen behavior seemed to be different depending on the pore diameter of the substrate. However, closer observation showed that the initial morphology observed in the smaller pore diameter substrates could also be found in the rest of the substrates. Those areas of larger pore diameter substrates where there is a larger contact area for the collagen to support itself showed a similar collagen morphology than the previous substrates.

After the collagen behavior has been addressed regarding its behavior, the next question that was studied was whether the collagen layer masks the surface roughness of the substrate used for PC12 cell culture. To fully answer it, the surface roughness (Sa) in all substrates used for PC12 cell culture was determined with and without collagen. A t-test was performed between the two conditions of the substrate, and no statistical significance, $p<0.05$ (*), was found (Figure 29).

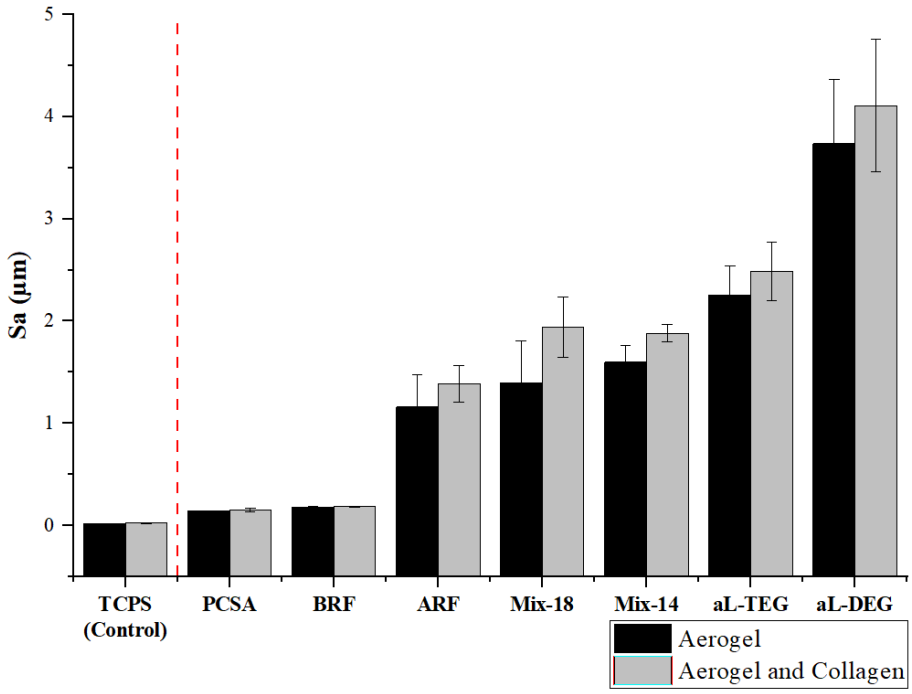

Figure 29: Surface roughness of all substrates with and without collagen. Surface roughness measured to show that coating the substrates with collagen does not change the underlying surface roughness of the substrate.

5.4 Material Properties of Aerogel Substrates

The material properties of the various substrates used for cell culture were measured to add a deeper understanding of the cell behavior on the different aerogel substrates. At the end of this section, a summary of all the features is shown where the different aerogels are compared with each other and to the control (TCPS). Pore diameter, surface roughness (Sa), and Young's modulus were measured for each substrate. As shown in Figure 29, surface roughness was measured with and without collagen to understand that the collagen layer does not mask the topography of the substrate. Similarly, the Young's modulus of the substrates was measured in two different conditions, after being submerged in medium for 24hrs at 37°C as well as a control, where the substrate was not immersed. To adequately address how PC12 cells react to the stiffness of the material, it is essential to focus on Young's modulus measured in similar

conditions as the cell culture. Therefore the difference between those two conditions is significant.

5.4.1 Material Properties of (PCSA)

The first main material property of PCSA that was observed during cell culture was the structure of the aerogel by means of SEM imaging. The pore diameter of the PCSA is in the nanometer range, and therefore the pores of the substrate are not visible when imaging cells, but it is shown in the form of surface roughness. The surface roughness of the PCSA was measured. As it has been mentioned in chapter 2, section 2.4.3, the topography of the substrates was measured using the surface roughness (Sa). PCSA was measured to have a larger surface roughness than the control (TCPS), showing an order of magnitude difference between those two substrates. Moreover, in comparison to the control (TCPS), PCSA was found to be softer by 1MPa.

5.4.2 Material Properties of the BRF-CA

BRF-CA was also subjected to the same material properties tests described previously. When comparing the structure of the BRF-CA to PCSA, the pore diameter and surface roughness had similar scale values. Pore diameter was determined to be at the nanoscale, just like with PCSA.

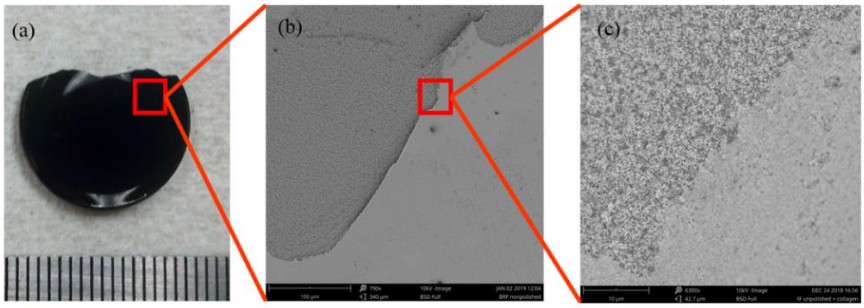

Figure 30: BRF-CA structure. (a) Macroscopic image of the aerogel with a reference bar of micrometers. (b) SEM image of BRF-CA with a reference bar of 100µm. (c) SEM image of BRF-CA with a reference bar of 10µm.

When observing the cell behavior at a larger magnification, the pore diameter is not observable, and it translates into a small surface roughness. Likewise, the surface roughness was measured and compared to the control (TCPS). BRF-CA was found to have a similar Sa to the PCSA, with a magnitude of difference with the control. Moreover, the measured Young's modulus of BRF-CA was found to be 3MPa lower than the control, and 2MPa lower than the PCSA. Even though both PCSA and BRF-CA have similar morphologies and topographies, there is a difference in Young's modulus.

It is important to note that BRF-CA and PCSA are similar substrates regarding their Young's modulus and surface roughness, but differ in their conductive properties. An experiment regarding electrical current in PCSA has been previously published [32] . Currently, a similar study has been performed where cell properties cultured in BRF-CA with and without an electrical bias are compared. Furthermore, this future study can be compared to the previous study regarding PCSA. Therefore, the conductive properties could be very well be isolated from the topography and stiffness.

5.4.3 Material Properties of the ARF-CA

ARF-CA was observed to have a unique structure compared to previous aerogel substrates. The ARF-CA structure was easily observed as a chain of beads connected, leaving voids between different chains that formed the pores (Figure 31).

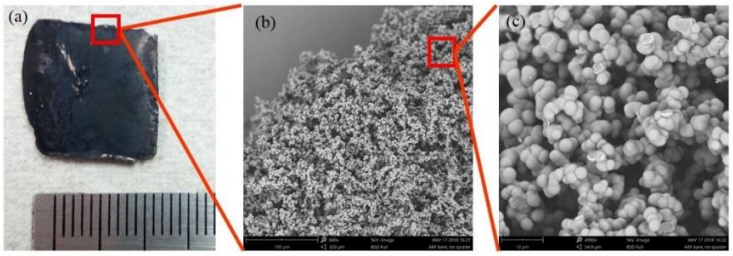

Figure 31: ARF-CA structure. (a) Macroscopic image of the aerogel with a reference bar of micrometers. (b) SEM image of ARF-CA with a reference bar of 100µm (c) SEM image of BRF-CA with a reference bar of 10µm.

The pore diameter was measured and determined to be larger than 10 µm, bringing a complete order of pore diameter compared to previous substrates. The measurement of surface roughness confirmed the difference in structure observed. ARF-CA Young's modulus was also measured and found to be similar to BRF-CA. Consequently, the ARF-CA substrate has a different topography but similar young's modulus compared to the other CA substrate, BRF-CA. Likewise to the conductivity of BRF-CA, ARF-CA can also be used to understand the electric stimulation to a conductive substrate as compared to a dielectric.

5.4.4 Material Properties of the MSPA Mix-14

The MSPA Mix-14 was tested to understand its materials properties. When Mix-14 was observed using the SEM, the pore diameter and structure were determined to be quite different from previous substrates with the polymer chains visible at micrometer scales. Unlike ARF-CA, the structure of the aerogel was less similar to beads but of a continuous chain (Figure 32). The pore diameter was measured to be an in-between ARF-CA and BRF-CA, around 3µm. The stiffness of this aerogel was expected to be quite low, as it is a memory shape material. Therefore, Mix-14 is an aerogel substrate that bridges the structure and surface roughness of ARF-CA and the other two substrates (PCSA and BRF-CA) while bringing a different Young's modulus.

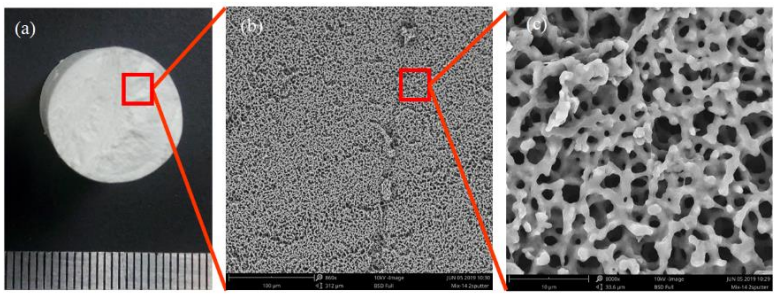

Figure 32: SMPA Mix-14 structure. (a) Macroscopic image of the aerogel with a reference bar of micrometers. (b) SEM image of SMPA Mix-14 with a reference bar of 100µm. (c) SEM image of BRF-CA with a reference bar of 10µm.

5.4.5 Material Properties of the MSPA Mix-18

Similar results were obtained regarding the MSPA Mix-18, as they were found in Mix-14. The pore diameter was found in the same range as Mix-14. The aerogel structure, surface roughness, and Young's modulus are similar to those of Mix-14 (Figure 33).

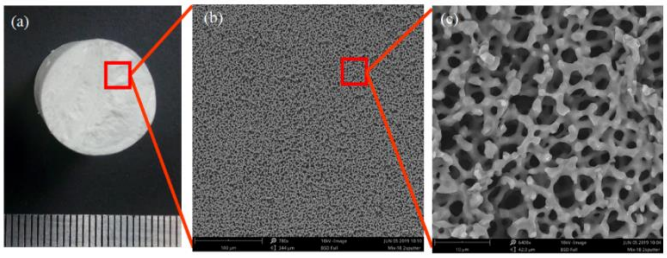

Figure 33: SMPA Mix-18 structure. (a) Macroscopic image of the aerogel with a reference bar of micrometers. (b) SEM image of SMPA Mix-18 with a reference bar of 100µm. (c) SEM image of BRF-CA with a reference bar of 10µm.

5.4.6 Material Properties of the MSPA aL-DEG

Another type of MSPA is aL-DEG. This type of aerogel substrate was first observed using SEM. The aerogel structure was found to be extremely similar to that of the ARF-CA, which can be described as large beads connected, forming polymer chains (Figure 34). Moreover, the Young's modulus was expected to be found lower than the control and the non-memory shape aerogels. Even more, the stiffness of aL-DEG was found to be even lower than the previous MSPA substrates. AL-DEG was measured to have an order of magnitude lower than Mix-14 and Mix-18. Consequently, this substrate allows for a similar surface roughness and pore diameter of ARF-CA while showing a different range of Young's modulus.

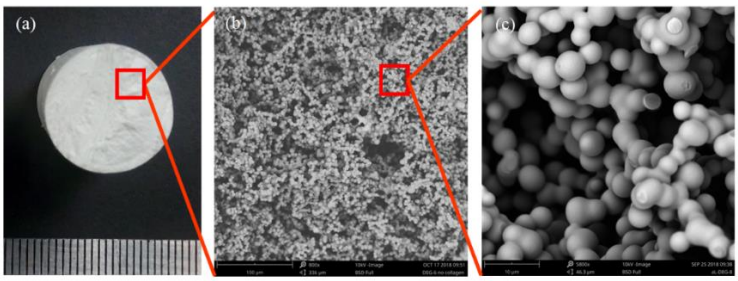

Figure 34: MSPA aL-DEG structure. (a) Macroscopic image of the aerogel with a reference bar of micrometers. (b) SEM image of SMPA aL-DEG with a reference bar of 100µm. (c) SEM image of BRF-CA with a reference bar of 10µm.

5.4.7 Material Properties of the MSPA aL-TEG

The MSPA aL-TEG properties were also measured and studied. The structure of this substrate was similar to Mix-14 and Mix-18 (Figure 35). This type of aerogel substrate allows for an in-between pore diameter compared to the other SMPA, with a pore diameter larger than the Mix-14 and Mix-18 but lower than the aL-DEG. The Young's modulus of this aerogel substrate was found to be like aL-TEG. Therefore, this substrate allows a comparison with aL-DEG where the Young's modulus is similar, but the structure and surface roughness is different.

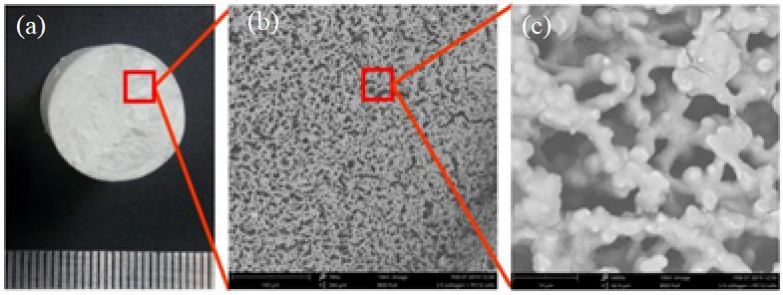

Figure 35: SMPA aL-TEG structure. (a) Macroscopic image of the aerogel with a reference bar of micrometers. (b) SEM image of SMPA aL-TEG with a reference bar of 100µm. (c) SEM image of BRF-CA with a reference bar of 10µm.

5.4.8 Summary of all Aerogel Material Properties

The different material properties of the aerogels used for PC12 cell substrate are key to further understand how cell behavior responds to materials' properties. As mentioned, three different properties were measured, pore diameter, surface roughness, and Young's modulus. Pore diameter is described in Figure 36, where the substrates have been plotted with increasing pore diameter. Both PCSA and BRF-CA substrates have similar pore diameters in the nanoscale. The control (TCPS), a non-porous substrate, was labeled to have a value of zero. Mix-14 and Mix-18 have a similar pore diameter around 2µm, while ARF-CA and the memory shape aL-DEG have similar pore diameters above 10µm. The last memory shape aL-TEG is found between the two different groups of memory shape aerogels.

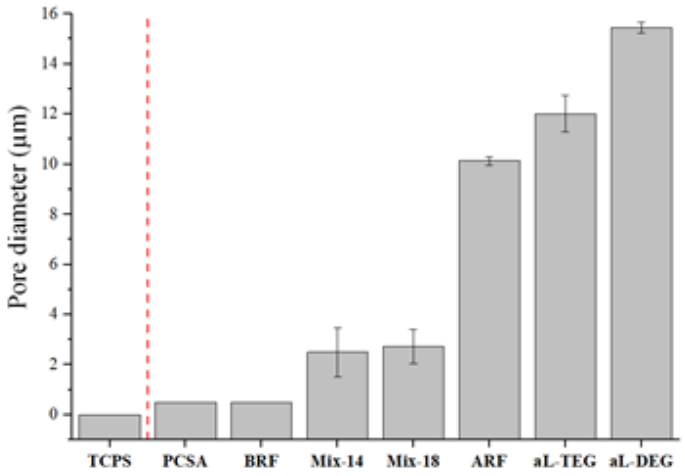

Figure 36: Aerogel's and control (TCPS) plotted with increasing pore diameter. Control (left) and aerogel (right of the red dotted line) have been plotted with increasing pore diameter. TCPS was assumed to be zero due to the lack of porosity.

The next material property measured for the aerogel substrates is surface roughness. The summary of all surface roughness of each substrate can be found in Figure 37. Profilometer images of each substrate's surface roughness can be found in Figure 38.

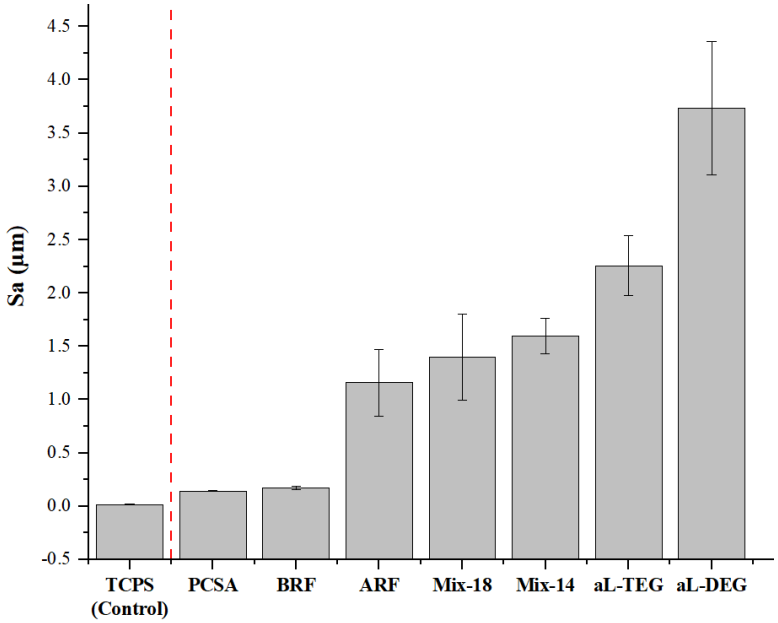

Figure 37: Distribution of the different substrates' surface roughness (Sa). The multiple substrates used for PC12 cell culture have been plotted as a function of increasing surface roughness (Sa)

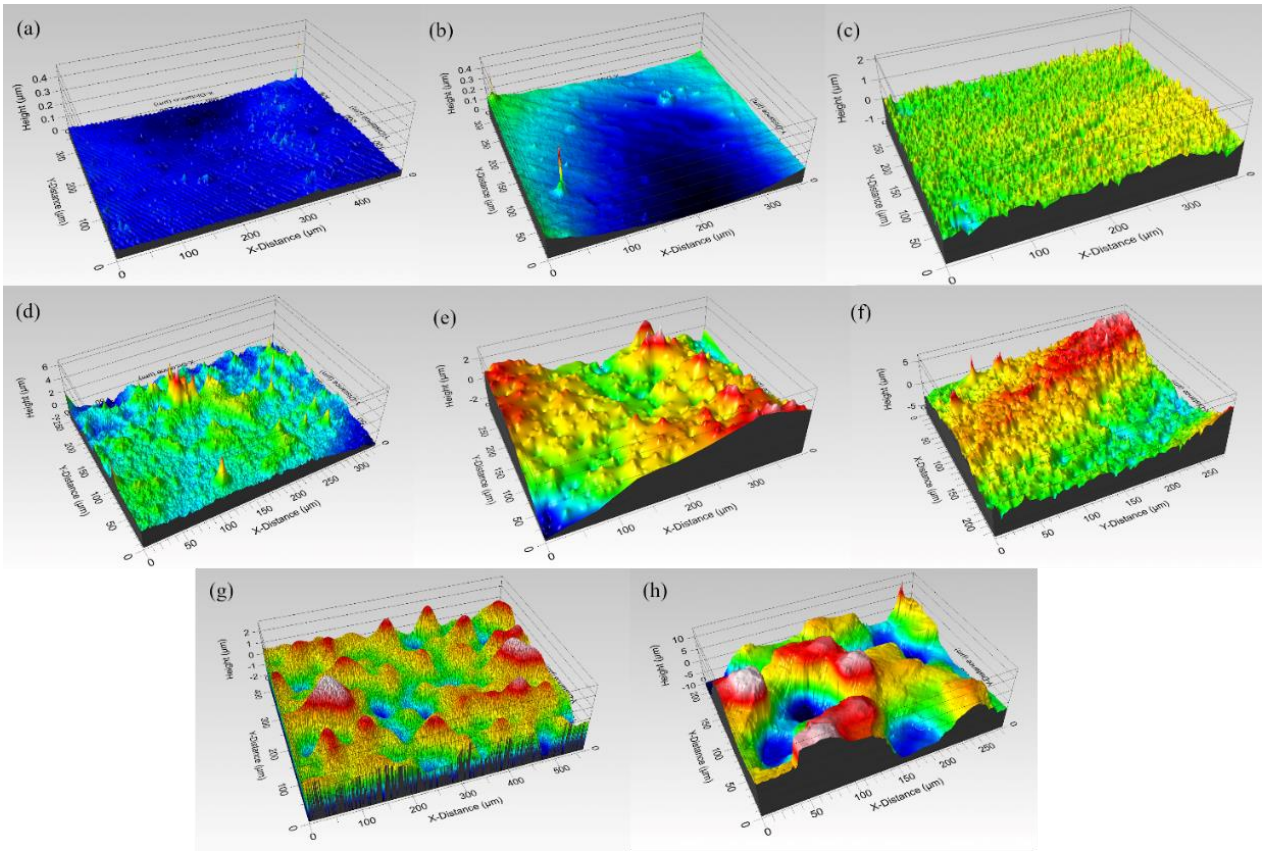

Figure 38: Profilometer images of the substrates' topographies with increasing surface roughness. Surface roughness of (a) TCPS (Control), (b) PCSA, (c) BRF-CA, (d) ARF-CA, (e) Mix-18 SMPA, (f) Mix-14 SMPA, (g) aL-TEG SMPA, (h) aL-DEG SMPA.

Moreover, similar similarities can be found in the surface roughness graph as it was found in the pore diameter. PCSA and BRF-CA substrates have similar pore diameters, in the nanometer size, and have similar topography in the nanometer height. On the other side of the spectrum, the SMPA aL-DEG and aL-TEG have the larger pore diameter and the higher surface roughness (Sa).

Finally, the last material property measured for the aerogel substrates for PC12 cell culture was their Young's modulus. In this case, the aerogel substrates were measured in two different conditions, as received or synthesized and after 24hrs of being submerged in cell culture medium at 36°C. A student's t-test was performed to determine the p-value between each substrate in the two conditions tested for. The majority of substrates showed a $p > 0.05$, and

therefore it was concluded that there was no difference between the Young's modulus between the substrate when submerged or not. The summary of all the measurements can be found in Figure 39.

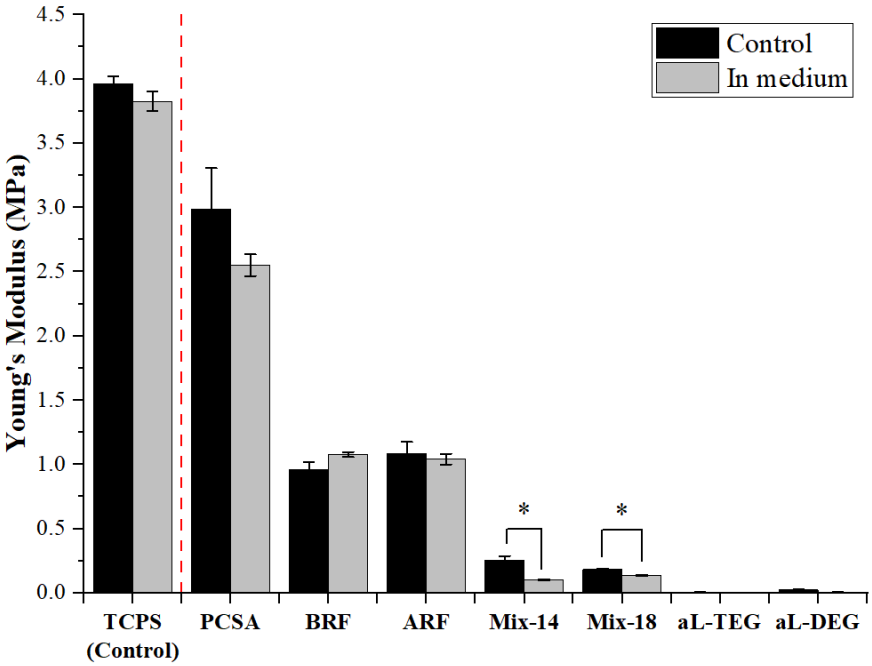

Figure 39: Distribution of the different substrates' Young's modulus (MPa). In black, the stiffness was measured at room temperature without submerging the aerogel; in grey, the aerogel was immersed in cell culture medium for 24hrs at 36°C.

5.5 Relating material properties and cell behavior

Until this point, the results regarding the material properties of the substrates used for cell culture have been shown, as well as the different cell behavior of the PC12 cells cultured on those substrates. In this section, the neurite length measured in all substrates is compared to the surface roughness (Sa) (Figure 40a) and Young's modulus (Figure 40b). Neurite length and surface roughness are compared, plotted, and fitted using a Gaussian fit in Origin9, where the optimum surface roughness is found around 500nm for neurite regeneration. Similarly, neurite length observed in the different aerogel substrates and control is plotted into the respective

Young's modulus of those substrates. The data is plotted and fitted with a cubic polynomial in origin, showing an optimum Young's modulus of 2MPa for neurite regeneration.

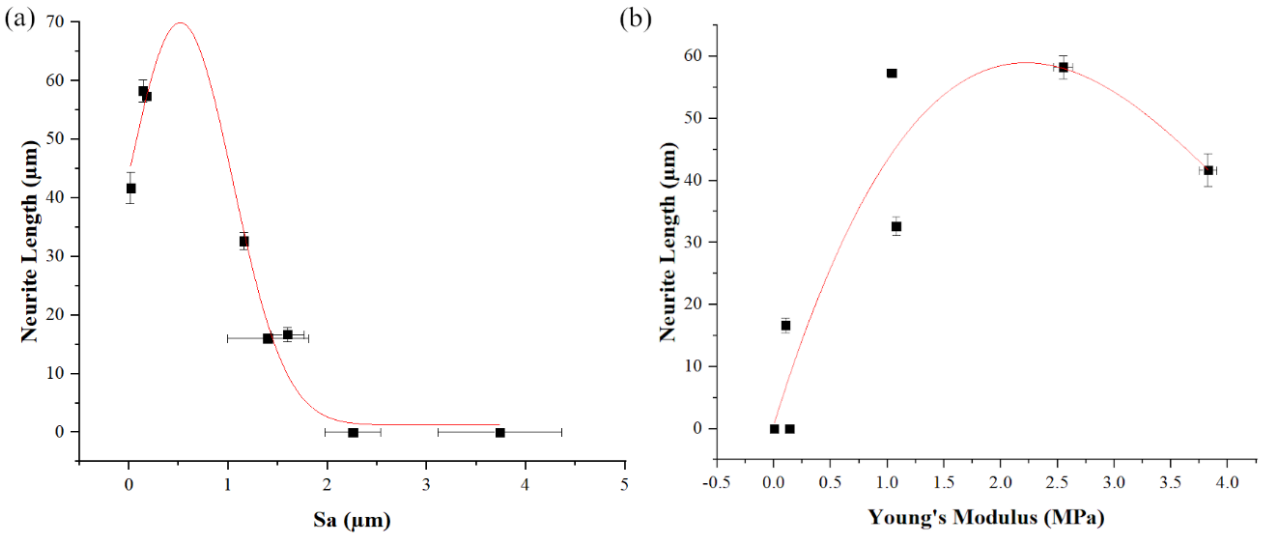

Figure 40: Neurite length as a function of material properties (a) Neurite length as a function of surface roughness with a gaussian fit, R^2 of 0.961. (b) Neurite length as a function of Young's modulus with cubic fit, R^2 of 0.801.

Chapter 6. Results and Discussion: Plasmonic Photo-Patterning on Aerogels

6.1 Successful transfer of pattern onto aerogel substrates

Polyurea crosslinked silica aerogels were successfully patterned by means of a plasmonic photo-patterning technique. This was confirmed by performing phase contrast microscopy and scanning electron microscopy on aerogels after the patterning step had been completed. Effective culture of PC12 cells on patterned aerogel substrates and glass (control) was also accomplished. Alignment of cells/ neurites to the pattern was concluded after performing analysis of the cell behavior and will be discussed in detail later in this chapter.

After one day (24 hrs) of cell culture, cells showed neurite outgrowth, indicating that the collagen-coated plasmonic photo-patterned aerogels are suitable substrates for neuronal scaffold applications and that the process is compatible and non-toxic. The uniformity and continuity of the polymer layer containing the pattern was evaluated at different locations using SEM and profilometry techniques on both the aerogel and the glass substrates. Figure 41a shows an image of the boundary between the plasmonic photo-pattern and the substrate over approximately a 200 nm range. The height of the plasmonic photo-pattern edge was measured at different points. A representative measurement is shown in Figure 41b, where a “step height” measurement is taken at the location indicated by the green and red markers of Figure 41a. Furthermore, the SEM analysis of the boundaries concurs with the uniformity and continuity results inferred from the profilometry images of Figure 41c.

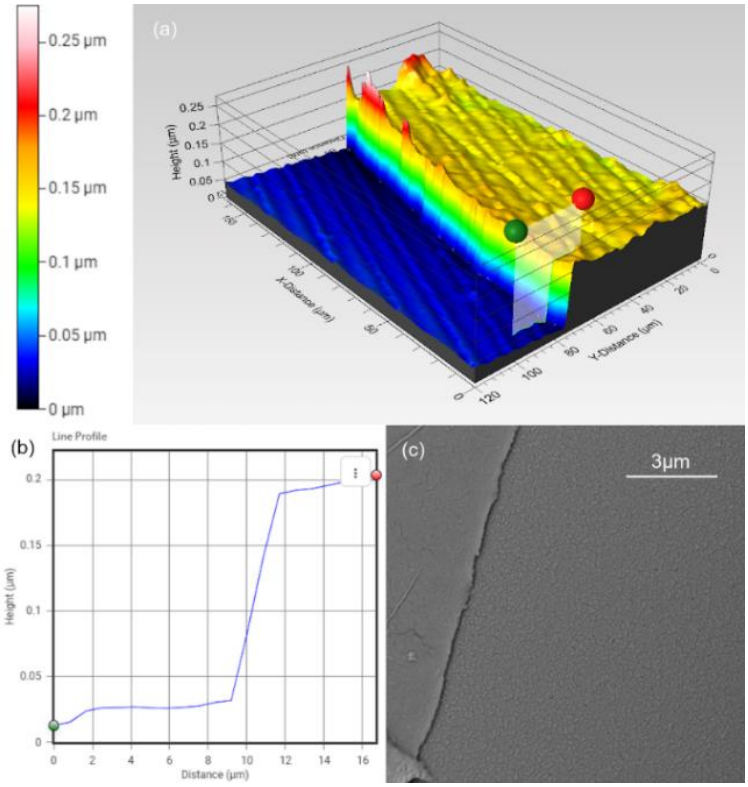

Figure 41: Imaging of plasmonic photo-pattern. (a) Profilometry image of the plasmonic photo-pattern border. (b) Step height measurement. (c) SEM image of the plasmonic photo-pattern boarder.

6.2 Neurite alignment in Plasmonic Photo-patterned Substrates

When evaluating the response of the PC12 cells to plasmonic photo-patterned substrates, it was determined that the cells do indeed follow some degree of alignment with the pattern underneath (Figure 42). Initially, the response of PC12 cells to a glass or aerogel substrate lacking any patterning was evaluated. Results show that the distribution of neurites, as expected, does not have a preference in orientation (Figure 42a, 42e, and blue traces in 42e and 42f). However, PC12 cells grown on patterned glass and aerogel substrates show a preferred direction of alignment. This alignment is consistent with the pattern on the substrates (Figure 42b, 42d, and red traces in 42e and 42f).

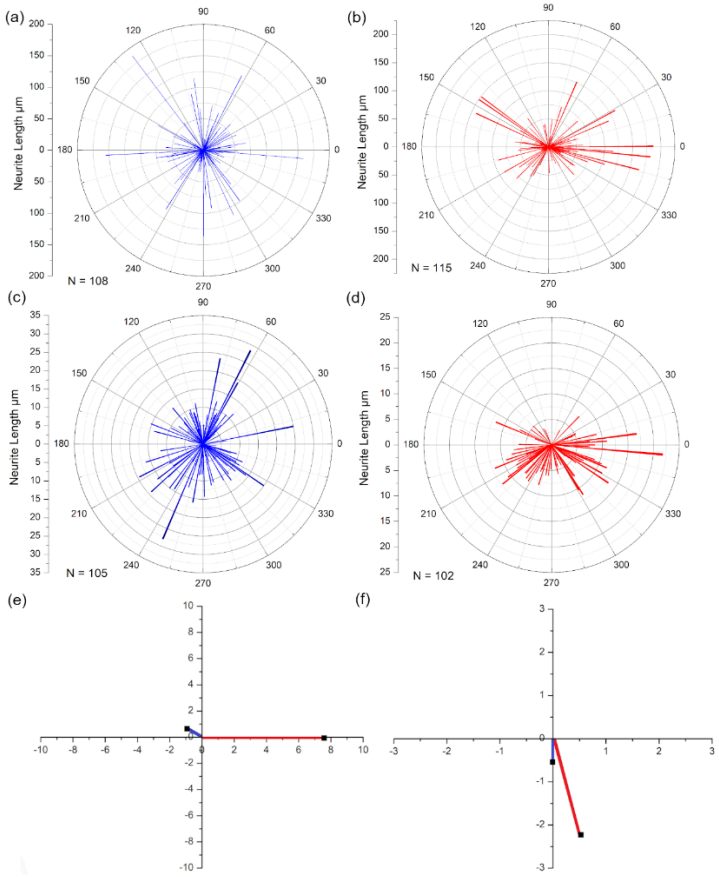

Figure 42: Neurite orientation (a) in glass (control) (b) in PCSA (control) (c) Glass with a plasmonic pattern (c) PCSA with a plasmonic pattern (e) Average neurite orientation in glass without (blue) and without a plasmonic pattern (red) (f) Average neurite orientation in PCSA without (blue) and without a plasmonic pattern (red).

Chapter 7. Conclusion and Future Works

This body of work focuses on understanding the effect of material properties on the behavior of PC12 neurons and how these reponses can be utilised to (a) understand cell mechanisms and (b) design neural prosthetics that can deliver the desired outcome. The first part of the work attemepted to quantify the relationships between cell behavior and substrate properties, while the second part investigated the feasibility of creating precise patterns on aerogel susbtrates for alignment by means of plasmonic photopatterning techniques.

It was previously shown that PC12 cells grow longer extensions on aerogel susbtrates when compared to their response on control susbtrates. However, it was not a comprehensive study and only one type of aerogel was explored. The work presented here investigated the response of PC12 cells to aerogels with different pore structures and different Young's moduli, presenting a comprehensive analysis of the findings. Key cell properties such as neurite length and orientation were studied and quantified. Results showed an optimum range for substrate stiffness and pore structure that lead to the fastest regeneration rate on aerogels. Topographies with a Sa of the order of 0.5 μm demosntrated an increased neurite outgrowth while Young's moduli in the range 1-3MPa support the fastest neurite regeneration rate. Therefore, based on the results of this study, random topographies with surface roughness of 0.5 μm and Young's modulus of 2MPa are the optimum substrates for neurite outgrowth in PC12 cells.

Other key cell properties were also impacted by the substrate properties. A decrease in neurite density was observed for all experiments performed on aerogels. Furthermore, the cell contact area was found to decrease with lower stiffness and higher surface roughness. Those results have shown a degree of alignment in neurites due to the continuous topography. Further investigations are needed.

Future steps for this work should consist of using more aerogel substrates with different materials properties from the ones used in this study — for example, SMPAs with smaller surface roughness similar to those of PCSA. On the other hand, further investigation of the plasmonic photo-patterning of aerogels should be performed. This part of the experiments would help further align and enhance neurite outgrowth. The alignment of neurites is essential due to the nature of peripheral nerve repair.

References

[1] G. G. Matthews, Introduction to neuroscience, Malden: Blackwell Science, 2000.

[2] I. B. Levitan and L. K. Kaczmarek, The neuron: cell and molecular biology, New York: Oxford University Press, 1991.

[3] American Society for Surgery of the Hand, "Nerve Injuries," [Online]. Available: www.handcare.org.

[4] S. R. Cajal, "Degeneration and Regeneration of the Nervous System," *Oxford University Press,* 1928.

[5] X. Navarro , "Functional Evaluation of Peripheral nerve regeneration and target reinnervation in animal models: A critical overview," *European Journal of Neuroscience,* vol. 43, no. 3, pp. 271-286, 2016.

[6] E. Armantrout, "Nerve Conduction Studies and Needle Electromy," in *Orthopaedic Physical Therapy Secrets*, Elsevier Inc., 2017, pp. 135-139.

[7] L. Parhamifar, H. Andersen, L. Wu, A. Hall, D. Hudzech and S. M. Moghimi, "Polycation-Mediated Integrated Cell Death Processes," in *Advances in Genetics*, Elsevier Inc, 2014, pp. 353-398.

[8] A. de Lahunta and E. Glass, "Lower Motor Neuron: Spinal Nerve, General Somatic Efferent System," in *Veterinary Neroanatomy and Clinical Neurology*, Elsevier Inc., 2009, pp. 77-133.

[9] D. Purves, G. J. Augustine and D. Fitzpatrick, "The Axonal Growth Cone," in *Neuroscience*, Sunderland, Sinauer Associates, 2001.

[10] G. Lundborg, "Nerve injury and repair - a challenge to the palstic brain," *Journal of the Peripheral Nervous System,* vol. 8, no. 4, pp. 209-226, 2003.

[11] C. A. Taylor, D. Braza, J. B. Rice and T. Dillingham, "The incidence of peripheral nerve injury in extremity trauma," *The American Journal of Physical Medicine and Rehabiliation,* vol. 87, no. 5, pp. 381-385, 2008.

[12] B. J. Pfister, T. Gordon, J. R. Loverde, A. S. Kochar and S. E. Mackinnon, "Biomedical engineering strategies for peripheral nerve repair: surgical applications, state of the art, and future challenges," *Critical Reviews in Biomedical Engineering,* vol. 39, no. 2, pp. 81-124, 2011.

[13] D. Gigo-Benato, T. L. Russo, S. Geuna , N. R. Dominiques, T. F. Salvini and N. A. Parizotto, "Elextrical stimulation Impairs Early Functional Recovery and Accentuates SKeletal Muscle Atrophy after Sciatic Nerve Crush Injury in Rats," *Muscle Nerve,* pp. 685-693, 2010.

[14] S. K. Lee and S. W. Wolfe, "Peripheral nerve injury and repair," *Journal of the American Academy of Orthopaedic Surgeons,* vol. 8, no. 4, pp. 243-252, 2000.

[15] C. Krarup, M. Boeckstyns, A. Ibsen, M. Moldovan and S. Archivald, "Remodeling of motor units after nerve regeneration studied by quantitative electromyography.," *Clinical Neurophysiology,* vol. 2, p. 127, 1675-1682.

[16] P. Mafi, S. Hindocha, M. Dhital and M. Saleh, "Advances of Peripheral Nerve Repair Techniques to Improve Hand Function: A systematic Review of Literature," *The Open Orthopedics Journal,* pp. 60-68, 2012.

[17] C. E. Schmidt, V. R. Shastri, J. P. Vacanti and R. Langer, "Stimulation of neurite outgrowth using an electrically conducting polymer," *Proceedings of the National Academy of Sciences,* 1997.

[18] J. K. Terzis, D. D. Sun and P. K. Thanks, "Historical and Basic Science Reveiw: Past, Present and Future of Nerve Repair.," *Reconstructive Microsurgery,* pp. 215-225, 1997.

[19] S. Geuna, P. Tos and B. Battiston, Essays on peripheral nerve repair and regeneration, New York: Elsevier/Academic Press, 2009.

[20] C. Simitzi, A. Ranella and E. Stratakis, "Controllng the morphology and outgrowth of nerve and neuroglial cells: The effect of surface topography," *Acta Biomaterialia,* vol. 51, pp. 21-52, 2017.

[21] S. Bai, H. Han, X. Huang, W. Xu, D. L. Kaplan, H. Zhu and Q. Lu, "Silk scaffolds with tunable mechanical capability for cell differentiation," *Acta Biometarialia,* vol. 20, pp. 22-31, 2015.

[22] J. P. Mather and P. E. Roberts, Introduction to Cell and Tissue Culture: Theory and Technique, Springer Science and Business Media, 2007.

[23] G. Kaur and J. M. Dufour, "Cell lines," *Spermatogenesis,* vol. 2, no. 1, pp. 1-5, 2012.

[24] M. Gulino, D. Kim, S. Pane, S. D. Santos and A. P. Pego, "Tissue Response to Neural Implants: The use of Model Systems Toward New Design Solutions of Implantable Microelectrodes," *Front Neurosci,* vol. 13, no. 689, 2019.

[25] L. Greene and A. S. Tischler, "Establishment of noradrenergic clonal line of rat adrenal pheochromocytoma cells which respond to nerve growth factor," *Proc Natl Acad Sci USA,* vol. 73, no. 7, pp. 2424-2428, 1976.

[26] R. Akeson and S. L. Warren, "PC12 adhesion and neurite formation on selected substrates are inhibited by some glycosaminoglycans and fibronectin-derived tetrapeptide," *Exp Cell Res,* vol. 162, no. 2, pp. 347-62, 1986.

[27] R. Akeson and S. L. Watten , "Interactions of a neuronal cell line (PC12) with laminin, collagen IV, and fibronectin: idenification of integrin-related glycoproteins involved in attachment and process outgrowth," *Experimental Cell Research,* pp. 347-362, 1986.

[28] L. A. Flanagan, Y.-E. Ju, B. Marg, M. Osterfield and P. A. Janmey, "Neurite branching on deformable substrates," *Neuroreport,* vol. 13, no. 18, pp. 2411-2415, 2002.

[29] F. Haq, V. Anandan, C. Keith and G. Zhang, "Neurite development in PC12 cells cultured on nanopillars and nanopores with sizes comparable with filopodia," *Intrantional Journal of Nanomedicine,* pp. 107-115, 2007.

[30] A. Klymoc, C. T. Rodriguez Neves, J. te Riet, M. J. Agterberg, E. A. Mylanys, A. F. Snik, J. A. Jansen and F. X. Walboomers, "Nanogrooved Surface-Patterns induce cellular organization and axonal outgrowth in neuron-like PC12-Cells," *Hearning Research,* vol. 320, pp. 11-17, 2014.

[31] M. Lampin, R. Warocquier-Clerout, C. Legris, M. Degrange and M. F. Sigot-Luizard, "Correlation between substratum roughness and wettability, cell adhesion, and cell migration," *Biomedical Material Research,* vol. 36, no. 1, pp. 99-108, 1997.

[32] K. J. Lynch, O. Skalli and F. Sabri, "Growing Neural PC-12 Cell on Crosslinked Silica Aerogels Increases Neurite Extension in the Presence of an Electric Field," *Journal of Functional Materials,* vol. 9, no. 2, p. 30, 2018.

[33] M. A. Schwarz, M. Mitchell and D. L. Emerson, "Reconstituted Basement Membrane Enhances Neurite Outgrowth in PC12 Cells Induced by Nerve Growth Factor," *Cell Growth Differentiation,* p. 313, 1990.

[34] A. Rukenstein, R. E. Rydel and L. A. Greene, "Multiple agents rescue PC12 cells from serum-free cell death by translation- and transcription-independent mechanisms," *Journal of Neuroscience,* vol. 11, no. 8, pp. 2552-2563, 1991.

[35] J. Stergar and U. Maver, "Review of aerogel-based materials in biomadical applications," *J Sol-Gel Sci Technology,* vol. 77, pp. 738-752, 2016.

[36] I. Smirnova, S. Suttiruengwong and W. Arlt, "Feasibility study of hydrophilic and hydrophobic silica aerogels as drug delivery systems," *J Non-Cryst Solids,* vol. 350, pp. 54-60, 2004.

[37] W. Yin and D. A. Rubenstein, "Biomedical Applications of Aerogels," in *Aerogels Handbook*, Springer Science & Business Media,, 2011, pp. 683-694.

[38] R. M. Rajendar, A. M. Michael, S. Vasudha, S. Bano, R. R. Raj, C. K. Subhas and A. M. Mark, "Silk fibroin aerogels: potential scaffolds for tissue engineering applications," *Biomed Mater,* vol. 10, no. 3, 2015.

[39] T. H. Lu, Q. Li, W. S. Chen and H. P. Yu, "Composite aerogels based on dialdehyde nanocellulose and collagen for potential applications as wound dressing and tissue engineering scaffold," *Compos Sci Technol,* vol. 94, pp. 132-138, 2014.

[40] F. Sabri, J. A. Cole, M. C. Scarbrough and N. Leventis, "Investigation of polyurea-crosslinked silica aerogels as a neuronal scaffold: a pilot study," *PloS one,* vol. 7, no. 3, 2012.

[41] F. Sabri, J. D. Boughter Jr., D. Gerth, O. Skalli, T.-C. N. Phung, G.-R. M. Tamula and N. Leventis, "Histological Evaluation of the Biocompatibility of Polyurea Crosslinked Silica Aerogel Implants in a Rat Model: A Pilot Study," *PloS one,* vol. 7, no. 12, 2012.

[42] K. J. Lynch, O. Skalli and F. Sabri, "Investigation of surface topography and stiffness on adhesion and neurites extension of PC12 cells on crisslinked silica aerogel substrates," *PloS one,* vol. 12, no. 10, 2017.

[43] A. C. Pierre, "History of Aerogels," in *Aerogels Handbook*, Springer, 2011, pp. 3-20.

[44] A. Du, B. Zhou, Z. Zhang and J. Shen, "A Special Material or a New State of Matter: A Review and Reconsideration of the Aerogel," *Materials ,* vol. 6, no. 3, pp. 941-968, 2013.

[45] C. O. Urrutia, M. V. Dominguez-García, J. Flores-Estrada, A. Laguna-Camacho, J. Castillo-Cadena and M. V. Flores-Merino, "Mechanical Stimulation of Cells Through Scaffold Design for Tissue Engineering," *Scaffolds in Tissue Engineering - Materials, Technologies and Clinical Applications,* 2017.

[46] K. Franze and J. Guck, "The biophysics of neuronal growth," *Reports on Progress in Physics,* vol. 73, no. 9, 2010.

[47] C. Wu, "A Focal Point in Current Cell Biology and Molecular Medicine," *Cell Adhesion and Migration,* vol. 1, no. 1, 2007.

[48] N. Almouemen, H. M. Kelly and C. O'Leary, "Tissue Engineering: Understanding the Role of Biomaterials and Biophysical Forces on Cell Functionality Through Computational and Structural Biotechnology Analytical Methods," *Computational and Structural Biotechnology Journal,* vol. 17, pp. 591-598, 2018.

[49] R. Magno, V. A. Grieneisen and A. F. Maree, "The biophysical nature of cells: potential cell behaviours revealed by analytical and computational studies of cell surface mechanics," *MC Biophysics,* vol. 8, no. 8, 2015.

[50] Y. Yang, K. Wang, X. Gu and K. W. Leong, "Biophysical Regulation of Cell Behavior—Cross Talk between Substrate Stiffness and Nanotopography," *Engineering,* vol. 3, no. 1, pp. 36-54, 2017.

[51] M. E. Greenberg, L. A. Greene and E. B. Ziff, "Nerve growth factor and epidermal growth factor induce rapid transient changes in proto-oncogene transcription in PC12 cells.," *Journal of Biological Chemistry,* vol. 260, pp. 14101-14110, 1985.

[52] X. Zhou, A. Yang, Z. Huang, G. Yin, X. Pu and J. Jin, "Enhancement of neurite adhesion, alignment and elongation on conductive polypyrrole-poly(lactide acid) fibers with cell-derived extracellular matrix," *Colloids and surfaces B: Biointerfaces,* vol. 149, pp. 217-225, 2017.

[53] N. Leventis, "Polymer-Crosslinked Aerogels," in *Aerogels Handbook- Advances in Sol-Gel Derived Materials and Technologies*, New York, Springer, 2011.

[54] V. Karageorgiou and D. Kaplan, "Porosity of 3D biomaterial scaffold and osteogenesis," *Biomaterials,* vol. 26, no. 27, pp. 5474-5491, 2005.

[55] J. M. Zielinski and K. Kettle, "Physical Characterization: Surface Area and Porosity," Intertek, 2013.

[56] J. Fricke and T. Tillotson, "Aerogels: Production, characterization, and applications," *Thin Solid Films,* vol. 297, no. 1-2, pp. 212-223, 1997.

[57] J. Gurav, J. In-Keun, H.-H. Park, E. S. Kang and D. Nadargi, "Silica Aerogel: Synthesis and Applications," *Journal of Nanomaterials,* vol. 24, 2010.

[58] U. Schubert, "Chemistry and Fundamentals of the Sol-Gel Process," in *The Sol-Gel Handbook: Synthesis, Characterization, and Applications*, Wiley-VCH, 2015, pp. 3-28.

[59] C. J. Brinker, "Hydrolysis and condesation of silicates: effectos on structure," *Journal of Non-Crystalline Solids,* vol. 100, pp. 31-50, 1988.

[60] A. C. Pierre and G. M. Pajonk, "Chemistry of Aerogels and Their Applications," *Chem Rev,* vol. 102, pp. 4243-4265, 2002.

[61] F. J. O'Brien, B. A. Harley, L. J. Gibson and I. V. Yannas, "Influence of Pore Size on Cell Attachment in Collagen-Gag Scafolds," *Biomaterials,* vol. 26, no. 4, pp. 433-441, 2005.

[62] L. E. Bain, R. Collazo, S.-h. Hsu, N. P. Lathman and M. J. Manfra, "Surface topography and chemistry shape cellular behavior on wide band-gap semiconductors," *Acta Miomaterialia,* vol. 10, pp. 2455-2462, 2014.

[63] S. W. Moore and M. P. Sheetz, "Biophysics of substrate interaction: influence on neural motility, differentiation, and repair," *Dev. Neurobiol,* vol. 71, pp. 1090-1101, 2011.

[64] D. H. Kim, P. P. Provenzano, C. L. Smith and A. Levchenko, "Matrix nanotopography as a regulator of cell fultion," *J. Cell Biol,* vol. 197, pp. 351-360, 2012.

[65] D. Hoffman-Kim, J. Mitchel and R. Bellamkonda, "Topography, cell response, and nerve regeneration.," *Annual review of biomedical engineering,* vol. 12, pp. 203-231, 2010.

[66] H. Andersoon and A. Van der Berg, "Microfabrication and microfluidics for tissue engineering: state of the art and future opportunities," *Lab Chip ,* vol. 4, no. 2, pp. 98-103, 2004.

[67] N. R. Blumenthal, O. Hermanson, B. Heimrich and V. P. Shastri, "Stochastic nanoroughness modulates neuron-astrocyte interactions and fucntion via mechanosensiong cation channels," *Proc. Natl. Acad. Sci U.S.A,* pp. 16124-16129, 2014.

[68] ASME, "Surface texture," American Society of Mechanical engineers, New York, 1995.

[69] I. S. Yeo, "Surface modification of dental biomaterials for controlling bone response," in *Bone Response to Dental Implant Materials*, Woodhead Publishing, 2017, pp. 43-64.

[70] R. Leach, L. Brown, X. Jiang, R. Blunt, M. Conroy and D. Mauger, Measurement Good Practice Guide, National Physical Laboarotry, 2008.

[71] T. V. Vorburger, J. A. Dagata, G. Wilkening and K. Iizuka, "Caracterization of Surface Topography," in *Beam effects, surface topography, and debth profiling in surface analysis*, Kluwer Academic Publishers, 2002, pp. 275-350.

[72] R. Leach, "Introduction to Surface Texture Measurement," in *Optical Measurement of Surface Topography*, Springer, 2011, pp. 1-11.

[73] j. schmit, "white-light Inteference 3D Microscopes," in *handbook of Optical Dimensional Metrology*, CRC Press, 2016, pp. 395-418.

[74] J. Schmit, "3D White Light Interference Microscope with Specialized," in *Advanced Mechatronics Solutions*, Switzerland, Springer, 2016, pp. 553-558.

[75] Zygo, "Optical Profiler Basics," Amatek ultra precision technologies, [Online]. Available: https://www.zygo.com/?/met/profilers/opticalprofilersabout.htm.

[76] S. Tofighi, A. Bahrampour, N. Pishbin and A. R. Bahrampour, "Interferomic Fiber-Optic Sensors," in *Optical Fiber Sensors: Advanced Techniques and Applications*, CRC press, 2015, pp. 491-520.

[77] N. E. Dowling, Mechanical Behavior of Materials, Pearson Eduacation Limited, 2013.

[78] Y. S. Pek, A. Wan and J. Y. Ying , "The effect of matrix stiffness on mesenchymal stem cell differentiation in a 3D thixotropic gel," *Biomaterials,* vol. 31, pp. 385-391, 2010.

[79] N. D. Leipzig and M. S. Shoichet, "The effect of substrate stiffness on adult neural stem cell behaviour," *Biomaterials,* pp. 6867-6878, 2009.

[80] B. C. Isenberg, P. A. DiMilla, M. Walker, S. Kim and J. Y. Wong, "Vascular smooth muscle cell durotaxis depends on substrate stiffness gradient strenght," *Biophys J,* vol. 97, pp. 1313-1322, 2009.

[81] A. Engler, L. Bacakova, C. Newman, A. Hategan, M. Griffin and D. Discher, "Substrate compliance versus ligand desnity in cell on gel responses," *Biophys J,* vol. 86, pp. 617-628, 2004.

[82] N. D. Leipzig and M. S. Shoichet, "The effect of substrate stiffess on adult neural stem cell behavior," *Biomaterials,* vol. 30, pp. 6867-6878, 2009.

[83] A. Buxboim, K. Rajagopal, A. E. Brown and D. E. Discher, "How deeply eclls feel: methods for thin gels," *J Phys Condens Matter.,* vol. 22, no. 19, 2010.

[84] J. J. Licari and D. W. Swanson, "Test and Inspection Methods," in *Adhesives Technology for Electronic Applications*, Elsevier, 2011, pp. 345-378.

[85] E. J. Hearn, "Simple Stress and Strain," in *Mechanics of Materials Volume 1: An Introduction to the MEchancis of Elastic and Plastic Deformation of Solids and Structural Materials*, Butterworth Heinemann, 1997, pp. 1-26.

[86] N. Saba, M. Jawaid and M. T. H. Sultan, "An Overview of mechanical and physical testing of composite materials," in *Mechnaical and Physical Testing of Biocomposites, Fibre-Reinforced Composites and Hybrid Composites*, Woodhead Publishing, 2019, pp. 1-12.

[87] Y. J. Chang, C. M. Hsu, C. H. Lin, M. S. Cheng Lu and L. Chen, "Electrical stimulation promotes nerve growth factor-induced neurite outgrowth and signaling," *Biochimica et Biophysica Acta,* vol. 1830, pp. 4130-4136, 2013.

[88] J. T. Francis, B. J. Gluckman and S. J. Schiff, "Sensitivity of Neurons to Weak Electric Fields," *Neurosicence,* vol. 23, pp. 7255-7261, 2003.

[89] J. Beeckman, K. Neyts and P. J. Vanbrabant, "Liquid-crystal photonic applications," *Optical Engineering,* vol. 50, 2011.

[90] P. F. McManamon, P. J. Bos, M. J. Escuti, J. Heikenfeld, S. Serati, H. Xie and E. A. Watson, "A review of phased array steering for narrow-band electrooptical systems," *roceedings of the IEEE,* vol. 97, no. 6, pp. 1078-1096, 2009.

[91] P. Chen, W. Ji, B. Y. Wei, W. Hu, V. Chigrinov and Y. Q. Lu, "Generation fo arbitrary vector beams with liquid crystal polarization converters and vector-photoaligned q-plates," *Applied Physics Letters,* vol. 107, no. 24, 2015.

[92] B. Y. Wei, W. Hu, Y. Ming, F. Xu, S. Rubin, J. G. Wang, V. Chigrinov and Y. Q. Lu, "Generating switchable and reconfigurable optical vortices via photopatterning of liquid crystals," *Advanced materials,* vol. 26, 2014.

[93] K. Gao, H. H. Cheng, A. K. Bhowmik and P. J. Bos, "Thin-film pancharatnam lens with low f-number and high quality," *Optics express,* vol. 23, 2015.

[94] A. Niv, G. Biener, V. Kleiner and E. Hasman, "Propagation-invariant vectorial bessel beams obtained by use of quantized Pancharatnam-Bery phase optical elements," *Opt Lett,* vol. 29, 2004.

[95] D. Iqbal and M. H. Samiullah, "Photo-responsive shape-memory and shape-chanign liquid-crystal polymer networks," *Materlas,* vol. 6, no. 1, pp. 166-142, 2013.

[96] L. T. de Haan, C. Sanches-Somolinos, C. M. Bastiaansen, A. P. Schemnning and D. J. Broer, "Engineering of complex order and the macroscopic deformation of liquid crystal polymer networks," *angewandte Chemie,* vol. 51, no. 50, 2012.

[97] C. Peng, T. Turiv, R. Zhang, Y. Guo, S. V. Shiyanovskii, Q. H. Wei, J. de Pablo and O. D. Lavrentovich, "Controlling placement of nonspherical (boomerang) colloids in nematic cells with hotopatterned dirctor," *Journal of Physics: Condensed Matter,* vol. 29, 2017.

[98] C. Peng, Y. Guo, T. Turiv, M. Jiang, Q. H. Wei and O. D. Lavrentovich, "Patterning of Lyotropic Chromotic Liquid Crystals by Photoalignment with Photonic Metamasks," *Advanced Materials,* vol. 29, 2017.

[99] C. Peng, T. Turiv, Y. Guo, Q. H. Wei and O. D. Lavrentovich, "Command of active matter by topological defects and patterns," *Science,* vol. 354, no. 6314, pp. 882-885, 2016.

[100] P. van der Asdonk, H. C. Hendrikse, R. M. Fernandez-Castrano, D. Voerman, B. Ramakers, D. Lowik, R. P. Sijbesma and P. Kouwer, "Patterning of Soft Matter across Multiple Length Scales," *Advanced Functional Materials,* vol. 26, no. 16, 2016.

[101] C. Peng, Y. Guo, C. Conklin, J. Vinals, S. V. Shiyanovskii, Q. W. Wei and O. D. Lavrentovich, "Liquid crystals with patterned molecular orientation as an electrolytic active medium," *Physics Review E,* vol. 92, 2015.

[102] F. Sabri, J. A. Cole, M. C. Scarbrough and N. Leventis, "Investigation of Polyurea-Crosslinked Silica Aerogels as a Neuronal Scaffold: A Pilot Study," *PLoS ONE,* 2012.

[103] R. W. Pekala, "Organic Aerogels from the Polycondensation of Resorcinol with Formaldehyde," *Mater Sci,* vol. 24, p. 3221, 1989.

[104] X. P. Lu, O. Nilsson, J. Fricke and R. W. Pekala, "Thermal and Electrical-Conductivity of Monolithic Carbon Aerogels," *Appl Phys,* vol. 73, p. 581, 1993.

[105] M. A. Worsley and T. F. Baumann, "Carbon Aerogels," *Hanbook of Sol-Gel Science and Technology,* 2016.

[106] R. B. Borgens, A. R. Blight and M. E. McGinnis, "Functional recovery after spinal cord hemisection in guinea pigs: The effects of applied electric fields," *J. Comp. Neurol.,* vol. 296, pp. 634-653, 1990.

[107] S. Donthula, C. Mandal, J. Schisler, T. Leventis, M. A. B. Meador, C. Sotiriou-Leventis and N. Leventis, "Nanostructure-Dependent Marcus-Type Correlation of the Shape," *Appl. Mater. Interfaces,* vol. 10, pp. 23321-23334, 2018.

[108] A. Levi, S. Biocca, A. Cattaneo and P. Calissano, "The mode of action of nerve growth factor in PC12 cells," *Mol. Neurobiol,* vol. 2, pp. 201-226, 1988.

[109] M. M. Portier, P. Brachet, B. Croizat and F. Gros, "Regulation of Peripherin in Mouse Neuroblastoma and Rat PC 12 Pheochromocytoma Cell Lines," *Dev. Neurosci.,* vol. 6, pp. 215-226, 1983.

[110] A. Yuan, T. Sasaki, A. Kumar, C. M. Peterhoff, M. V. Rao, R. K. Liem, J. Julien and R. A. Nixon, "Peripherin Is a Subunit of Peripheral Nerve Neurofilaments: Implications for Differential

Vulnerability of CNS and Peripheral Nervous System Axons," *Journal of Neuroscience,* vol. 32, no. 25, pp. 8501-8508, 2012.

[111] Y. J. Chang, C. M. Hsu, C. H. Lin, M. C. Lu and L. Chen, "Electrical stimulation promotes nerve growth factor-induced neurite outgrowth and signaling," *Biochim. Biophys. Acta BBA Gen. Subj. ,* vol. 1830, pp. 4130-4136, 2013.

[112] S. Manivannan and S. Terakawa, "Rapid sprouting of filopodia in nerve terminals of chromaffin cells, PC12 cells, and dorsal root neurons induced by electrical stimulation," *J. Neurosci,* vol. 14, pp. 5917-5928, 1994.

[113] J. N. Tiwari, V. Vij, K. C. Kemp and K. S. Kim, "Engineered Carbon-nanomaterial-based electrochemical sensors for biomolecules," *ACS nano,* vol. 10, no. 1, pp. 46-80, 2015.

[114] K. R. Jankowski, K. J. Flannelly and L. T. Flannelly, "The t-test: An influental inferential tool in Chaplaincy and other healthcare research," *Journal of Health Care Chaplaincy,* vol. 24, pp. 30-39, 2018.

[115] M. Rodriguez Sala, C. Peng, O. Skalli and F. Sabri, "Tunable neuronal scaffold biomaterials through plasmonic photo-patterning of aerogels," *MRS Communications,* 2019.

[116] T. Atkins and M. Escudier, "Supercritical fluid," in *A Dictionary of Mechanical Engineering:*, Oxford University Press, 2013.

[117] T. Riss, "Is your MTT assay really the best choice," Promega Corporation website, 2017. [Online]. Available: http://www.promega.in/resoruces/pubhub/is-your-mtt-assay-really-the-best-choice. [Accessed 2018].

[118] N. Li., X. Zang, Q. Song, R. Su, Q. Zhang, T. Kong, L. Liu, G. Jin, M. Tang and G. Cheng, "The promotion of Neurite Sprouting and Outgrowth of Mouse Hippocampal cells in culture by graphene substrates," *Biomaterials,* vol. 32, no. 35, pp. 9374-9382, 2011.

[119] H. Maleki, L. Durães and A. Portugal, "An overview on silica aerogels synthesis and different mechanical reinforcing strategies," *Journal of Non-Crystalline Solids,* vol. 385, pp. 55-74, 2014.

[120] Y. Hanzawa, K. Kaneko, R. W. Pekala and M. S. Dresselhaus, "Activated carbon aerogels," *Langmuir,* vol. 12, no. 26, pp. 6167-6169, 1996.

[121] N. Leventis, C. Sotiriou-Leventis, G. Zhang and A. Rawashdeh, "Nanoengineering strong silica aerogels," *Nano letters,* vol. 2, no. 9, pp. 957-960, 2002.

[122] N. Leventis, "Three-dimensional core-shell superstructures: mechanically strong aerogels," *Accounts of chemical research,* vol. 40, no. 9, pp. 874-884, 2007.

[123] R. K. Willits and S. L. Skornia, "Effect of collagen gel stiffness on neurite extension," *BiomaterialsScience,* vol. 15, no. 12, pp. 1521-1531, 2004.

[124] F. J. O'Brien, "Biomaterials & Scaffolds for Tissue Engineering," *Mateirlas Today,* vol. 14, no. 3, pp. 88-95, 2011.

[125] X. Y. Zhang, G. Fang and J. Zhou, "Additively Manufactured Scaffolds for Bone Tissue Engineering and the Prediction of their Mechanical Behavior: A Review.," *Materials,* vol. 50, p. 10, 2017.

[126] L. Roseti, V. Parisi, M. Petretta, C. Cavallo, G. Desando, I. Bartolotti and B. Grigolo, "Scaffolds for Bone Tissue Engineering: State of the art and new perspectives," *Mater Sci Eng C Mater Biol Appl.,* vol. 78, pp. 1246-1262, 2017.

[127] S. P. Soundarya, A. H. Menon, S. V. Chandran and N. Selvamurugan, "Bone tissue engineering: Scaffold preparation using chitosan and other biomaterials with different design and fabrication techniques.," *Int J Biol Macromol.,* vol. 119, pp. 1228-1239, 2018.

[128] S. Bose, M. Roy and A. Bandyopadhyay, "Recent advances in bone tissue engineering scaffolds," *Trends Biotechnol.,* vol. 30, no. 10, pp. 546-554, 2012.

[129] S. E. Mackinnon and C. B. Novak, "Washington University in St. Louis, School of Medicine," March 2001. [Online]. Available: http://nerve.wustl.edu/.

[130] K. L. Colen, M. Choi and D. T. W. Chiu, "The interfascicular nerve grafting of the median and ulnar nerves," *Journal of Bone and Joint Surgery,* vol. 54, no. 4, pp. 727-750, 1972.

[131] P. Konofaos and J. P. Halen, "Nerve repair by means of tubulization: past, present, future"," *Journal of Reconstructuve Microsurgery,* vol. 29, no. 3, pp. 149-164, 2013.

[132] J. W. Griffin, M. V. Hogan, A. B. Chhabra and D. N. Deal, "Peripheral nerve repair and reconstruction," *Journal of Bone and Joint Surgery,* vol. 95, no. 23, pp. 2144-2151, 2013.

[133] J. M. Maloney, E. B. Walton, C. M. Bruce and K. Van Vliet, "Influence of finite thickness and stiffness on cellular adhesion-induced deformation of compliant substrata," *Physical Review E,* vol. 78, no. 4, 2008.

[134] D. Howard, L. D. Buttery, K. M. Shakesheff and S. J. Roberts, "Tissue engineering: strategies, stem cells and scaffolds," *Journal of Anatomy,* vol. 2013, pp. 66-72, 2018.

[135] X. Xu, A. E. Warrington, A. J. Bieber and M. Rodriguez , "Enhancing Central Nervous System Repair-The Challenges," *CNS Drugs,* vol. 25, no. 7, pp. 555-573, 2011.

[136] M. Lampin, R. Warocquier-Clerout, C. Legris, M. Degrange and M. F. Sigot-Luizard, "Correlation between substratum roughness and wettability, cell adhesion, and cell migration," *J Biomed Mater Res,* vol. 36, no. 1, pp. 99-108, 1997.

[137] L. J. Struble and X. Ji, "Rheology," in *Handbooks of Analytical tecchniques in Concrete Science and Technology*, William Andrew, 2001, pp. 333-367.

[138] K. Gao , H. Cheng, A. Bhowmik and P. Bos, "Thin-film Pancharatnam lens with low f-number and high quality.," *Optics express,* vol. 23, no. 20, p. 26086, 2015.

[139] A. Niv, G. Biener, V. Kleiner and E. Hasman, "Propagation-invariant vectorial Bessel beams obtained by use of quantized Pancharatnam–Berry phase optical elements.," *Optical Letters,* vol. 29, no. 3, p. 238, 2004.

[140] M. Nasrollahzadeh, M. Atarod, M. Sajjadi, S. M. Sajadi and Z. Issaabadi, "Plant-Meditated Green Synthesis of Nanostructures: Mechanisms, characterization and applications.," in *Interface Science and Technology*, Elsevier, 2019, pp. 1992-322.

[141] R. R. Mather, "Surface modification of texiles by plasma treatments," in *Surface Modification of textiles*, Woodhead Publishing, 2009, pp. 296-317.

[142] Y. Yan, "Metals for Biomedical DevicesTribology and tribo-corrosion testing and analysis of metallic biomaterials," in *Metals for Biomedical Devices*, Woodhead Publishing, 2010, pp. 178-201.

[143] s. Fu, F. Cheng, T. Tjahjowidodo, Y. Zhou and D. Butler, "A Non-Contact Measuring System for In-Situ Surface," *sensors,* vol. 18, no. 8, 2018.

[144] R. Artigas, "Imaging Confocal Microscopy," in *Optical Measurement of Surface Topography*, Berlin, Springer, 2011.

[145] P. Pavlicek and E. Mikeska, "White-light interferometer without mechanical scanning," *Optics and Lasers in Engineering,* vol. 124, 2020.

[146] S. Chandrasekaran, P. G. Campbell, T. F. Baumann and M. A. Worsley, "Carbon aerogel evolution: Allotrope, graphene-inspired, and," *J. Mater. Res.,* vol. 32, no. 22, 2017.

[147] S. Rotshenker, "Wallerian degeneration: the innate-immune response to traumatic nerve injury," *Journal of neuroinflammation,* vol. 8, no. 109, 2011.